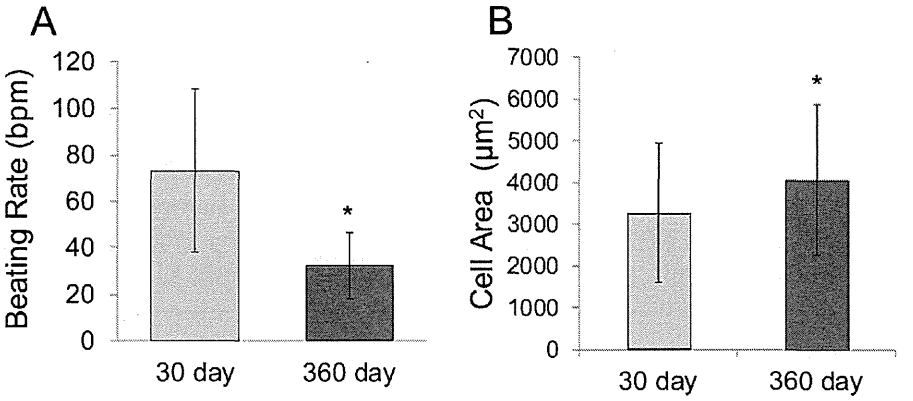

Figure 1. Comparison of human-induced pluripotent stem cell-derived cardiomyocytes (hiPSC-CMs) at 30 and 360 days after cardiac differentiation. (**A**) The rate of beating (beats/min [bpm]) of embryoid bodies (EBs) at 30 days was significantly higher than that of 360-day EBs (73.2±34.9 bpm vs. 32.2±14.2 bpm, P<0.0001). (**B**) Size of hiPSC-CMs increased significantly after long-term culture (3,277.4±1,679.5 μm^2 vs. 4,067.9±1,814.6 μm^2, P=0.01). *P<0.05 vs. 30-day.

maturation process and establish a protocol for creating homogeneous mature iPSC-CMs.

In this study, we investigated the ultrastructural, immunocytological, and gene expression changes of hiPSC-CMs in a long-term 2D culture. Here, we first report that mature sarcomeric structures with M-bands were detected only in 360-day hiPSC-CMs, which might be associated with lower expression levels of M-band-specific proteins compared with adult heart cells.

Methods

Culture of hiPSC and CM Differentiation

The hiPSC line 201B7 was retrovirally transfected with Oct3/4, SOX-2, Klf4, and c-Myc.[1,9] These lines displayed all the defining parameters[1] and the hiPSCs were maintained as described.[15]

We differentiated hiPSC-CMs as embryoid bodies (EBs).[16,17] In brief, hiPSCs aggregated to form EBs, and were cultured in suspension for 8 days. On day 8, the EBs were plated onto fibronectin-coated dishes and for the first 20 days, we followed the protocol as described previously.[16,17] Cultures were maintained in a 5% CO_2, 5% O_2, 90% N_2 environment for the first 12 days and then transferred into a 5% CO_2/air environment for the remainder of the culture period. At 20 days after cardiac differentiation, EBs were maintained in culture DMEM/F12 supplemented with 2% fetal bovine serum, 2 mmol/L L-glutamine, 0.1 mmol/L non-essential amino acids, 0.1 mmol/L β-mercaptoethanol, 50 U/ml penicillin, and 50 μg/ml streptomycin.[3] The medium was renewed every 2–3 days.

Immunocytochemistry

For immunostaining, single cells were isolated from microdissected 30- and 360-day-old beating EBs using collagenase B (Roche) and trypsin EDTA (Nacalai Tesque). The cells were plated onto fibronectin-coated dishes for 3 days to allow attachment. The cells were fixed in 4% paraformaldehyde and permeabilized in 0.2% Triton X-100 (Nacalai Tesque). The samples were stained with the following primary antibodies: rabbit polyclonal anti-cardiac troponin I (cTnI) (1:200; Santa Cruz), mouse monoclonal anti-myosin light chain 2a (MLC2a) (1:200; Synaptic Systems), rabbit polyclonal anti-myosin light chain 2v (MLC2v) (1:100; Proteintech Group), mouse monoclonal anti-βIII tubulin (1:100, Promega), mouse monoclonal anti-fibroblast (1:100, Acris Antibodies), and mouse monoclonal anti-human smooth muscle actin (1:100, Dako). We used the appropriate secondary antibodies: donkey anti-rabbit Alexafluor 594 (1:500, Invitrogen) and donkey anti-mouse Alexafluor 488 (1:500, Invitrogen). The nuclei were stained with DAPI (1:2000, Wako). The specimens were observed under a fluorescence microscope, Biozero BZ-9000 (Keyence), and the areas of cTnI-positive cells were calculated using a BZ-II analyzer (Keyence).

Transmission Electron Microscopy (TEM)

TEM was performed on 14-, 30-, 60-, 90-, 180-, and 360-day old EBs derived from hiPSC-CMs. EBs were microdissected and fixed for 1 h in 2% glutaraldehyde at 4°C in phosphate-buffered saline (PBS). All sections were treated with OsO_4 (1% for 1 min, and 0.5% for 20 min at 4°C) in PBS, dehydrated in ethanol and propylene oxide, and embedded in Luveak 812 (Nacalai Tesque). Ultrathin sections were cut with an ultramicrotome (Leica, Heidelberg, Germany) and observed with TEM (H-7650; Hitachi). All stages of EBs were examined in triplicate.

Analysis of mRNA Expression by Real-Time Quantitative Polymerase Chain Reaction (qPCR)

Total RNA was isolated using TRIzol Reagent (Invitrogen) from 20 to 30 EBs microdissected from 30-, 90-, 180-, and 360-day-old hiPSC-CMs, and treated with TURBO DNA-free Kit (Applied Biosystems). Total RNA from human heart tissue (left ventricle, left atrium, and fetal heart) was also reverse transcribed into complementary DNA (cDNA) for comparison. cDNA was synthesized from 1 μg of total RNA, in a total volume of 20 μl, using oligo $(dT)_{18}$ primer with Transcriptor First Strand cDNA Synthesis Kit (Roche). The PCR-related primers are detailed in **Table S1**. The real-time qPCR was performed using power SYBR Green PCR Master Mix (Applied Biosystems) for 6 samples. The expression of genes of interest was normalized to that of *GAPDH*. Relative quantification was calculated according to the $\Delta\Delta C_T$ method. The changes in gene expression levels were compared with those of hiPSC-

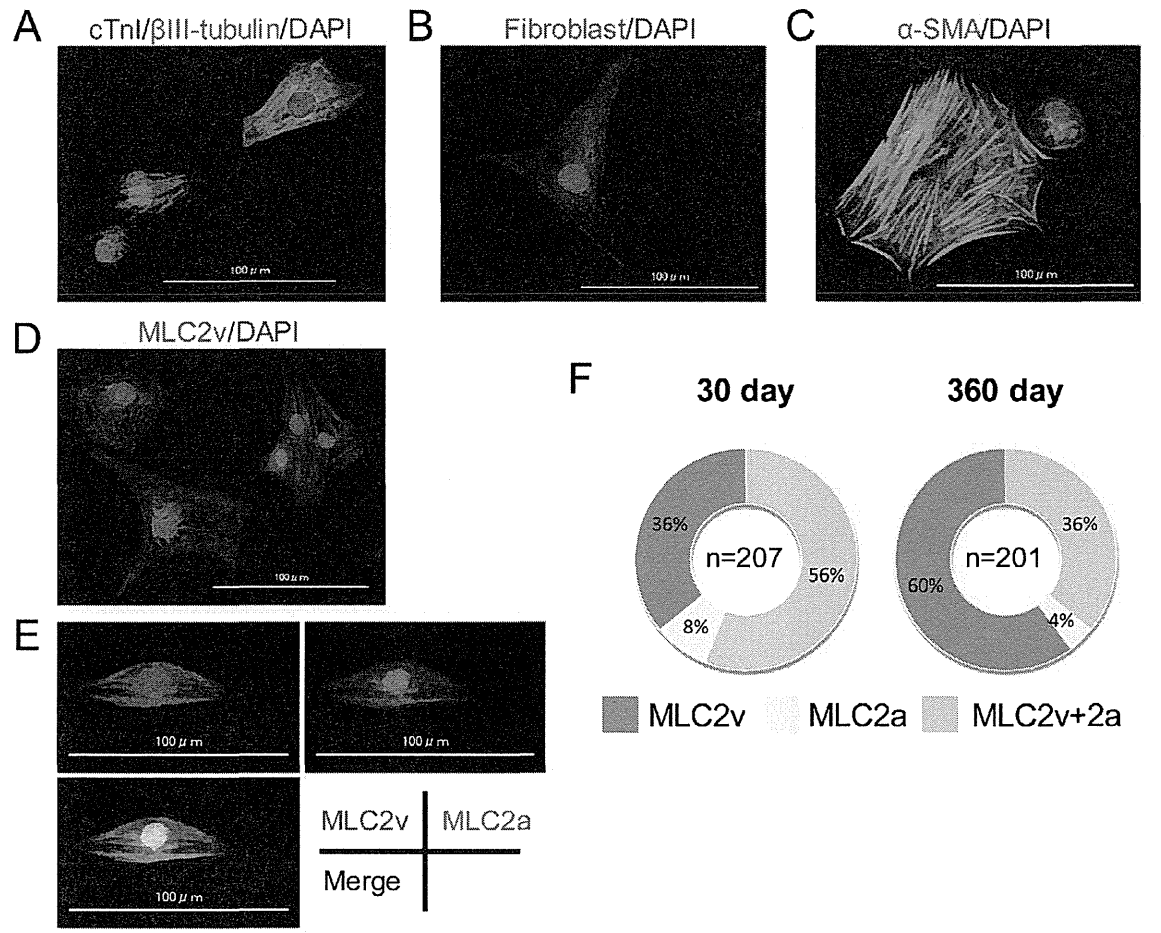

Figure 2. Immunostaining of human-induced pluripotent stem cell-derived cardiomyocytes (hiPSC-CMs) at 30 days after cardiac differentiation. (**A–E**) Immunostaining of single cells isolated from microdissected beating embryoid bodies (EBs) at 30 days using the following antibodies: (**A**) cTnI (red), βIII-tublin (green), and DAPI (blue); (**B**) fibroblast (green) and DAPI (blue); (**C**) α-SMA (green) and DAPI (blue); (**D**) MLC2v (green) and DAPI (blue); (**E**) MLC2v (red) and MLC2a (green). (**E**) hiPSC-CM expressing both MLC2v and MLC2a. (**F**) Properties of MLC2v-positive/MLC2a-negative, MLC2v-negative/MLC2a-positive, and MLC2v/MLC2a double-positive cells at 30 days and 360 days. Among the MLC2v- or MLC2a-positive cells, 36% of 30-day hiPSC-CMs were MLC2v-positive/MLC2a-negative mature ventricular CMs and 56% were MLC2v/MLC2a double-positive immature ventricular CMs. At day 360, MLC2v-positive/MLC2a-negative mature CMs increased to 60%, whereas MLC2v/MLC2a double-positive immature ventricular CMs decreased to 36%.

CMs at 30-day differentiation. The fold change is expressed as mean±SEM.

Statistical Analysis

All values are presented as mean±SEM. Statistical significance was evaluated by Student's t-test for 2 groups or 1-way analysis of variance followed by Tukey test for comparisons of multiple groups. Differences with $P<0.05$ were considered statistically significant.

Results

Long-Term Maintenance of hiPSC-CMs

Areas of spontaneous beating became visible as early as day 8 after differentiation, and kept beating for more than 360 days (**Movie S1**). The beating rate of 30-day-old EBs (n=42) was significantly higher than that of 360-day-old EBs (n=41; 73.2±34.9 beats/min vs. 32.2±14.2 beats/min, $P<0.0001$) (**Figure 1A**).

The size of dispersed hiPSC-CMs increased significantly after long-term culture as measured by their cell area (3,277.4±1,679.5 μm^2 vs. 4,067.9±1,814.6 μm^2, $P=0.01$) (**Figure 1B**).

Immunostaining Analysis of Beating EBs at 30 and 360 Days After Cardiac Differentiation

Immunostaining of single cells isolated by microdissected beating EBs detected cells positive not only for cTnI, MLC2v, and MLC2a, but also βIII-tubulin, fibroblasts, and α-SMA, suggesting the existence of neural cells, fibroblast-like cells, and vascular smooth muscle cells in the beating EBs as well as CMs (**Figures 2A–E**).

Among randomly selected single cells isolated from 30- (n=213) and 360-day-old (n=191) beating EBs, 61% and 64%, respectively, were positive for cTnI. Double immunostaining with anti-MLC2v and anti-MLC2a antibodies revealed that among the MLC2v- or MLC2a-positive cells, 36% were MLC2v-positive/MLC2a-negative, 8% were MLC2v-negative/

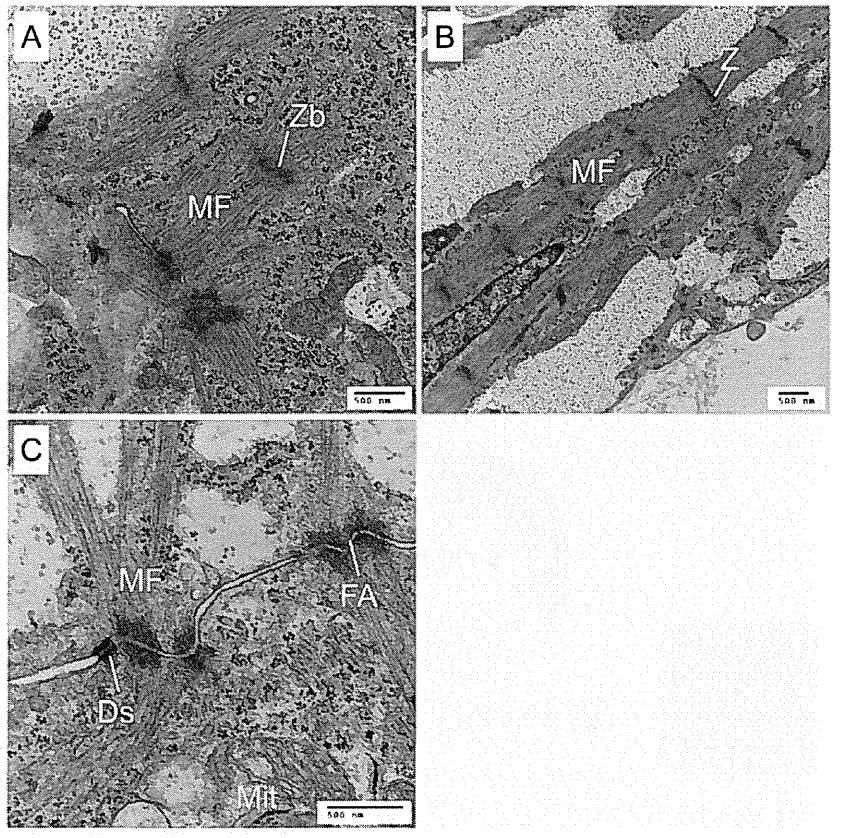

Figure 3. Transmission electron microscopy images of human-induced pluripotent stem cell-derived cardiomyocytes (hiPSC-CMs) at 14 days after cardiac differentiation. (**A**) hiPSC-CMs at 14 days contained myofibrils (MF) that lacked alignment or organized sarcomeric pattern. Scattered condensed Z-bodies (Zb) were also confirmed. (**B**) In some areas, a more developed pattern was noted in which myofibrils (MF) were held between a few of the Z-bands (Z). (**C**) CMs connected by desmosomes (Ds) and fascia adherens (FA) even at this early stage. Mitochondria (Mit) can be seen.

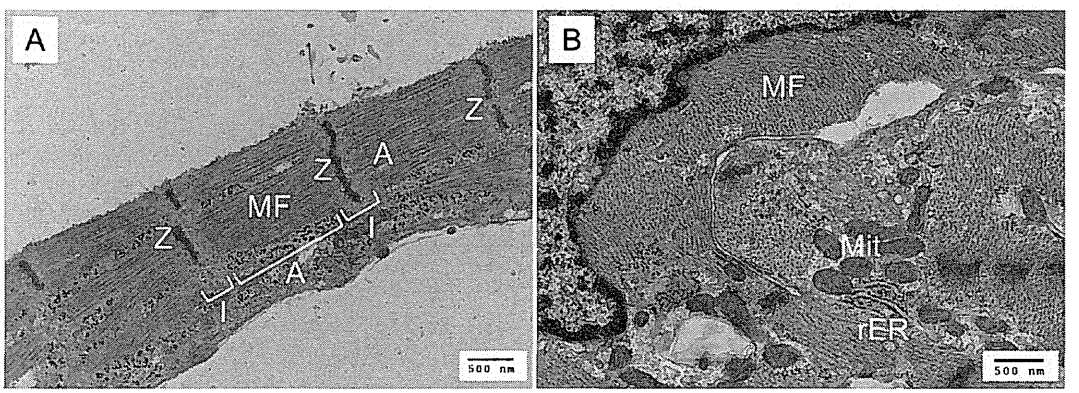

Figure 4. Transmission electron microscopy images of human-induced pluripotent stem cell-derived cardiomyocytes (hiPSC-CMs) at 30 days after cardiac differentiation. (**A**) hiPSC-CMs at 30 days appeared to be packed between parallel Z-bands. Some myofibrils (MF) showed A- (A) and I-bands (I). (**B**) Transverse section of sarcomere and rough endoplasmic reticulum (rER). Mitochondria (Mit) can be seen.

MLC2a-positive, and 56% were MLC2v/MLC2a double-positive CMs at 30-day differentiation. By day 360, MLC2v-positive/MLC2a-negative CMs increased to 60%, whereas MLC2v/MLC2a double-positive immature ventricular CMs decreased to 36% (**Figure 2F**).

Ultrastructural Analysis of hiPSC-CMs at 14-, 30-, 60-, 90-, 180-, and 360-Day Differentiation

hiPSC-CMs at 14-day differentiation contained myofibrils that lacked alignment or organized sarcomeric pattern, and were distributed diffusely in the cytoplasm in a disorganized fashion. Scattered patterns of condensed Z-bodies were also confirmed. However, in some areas, a more developed pattern was

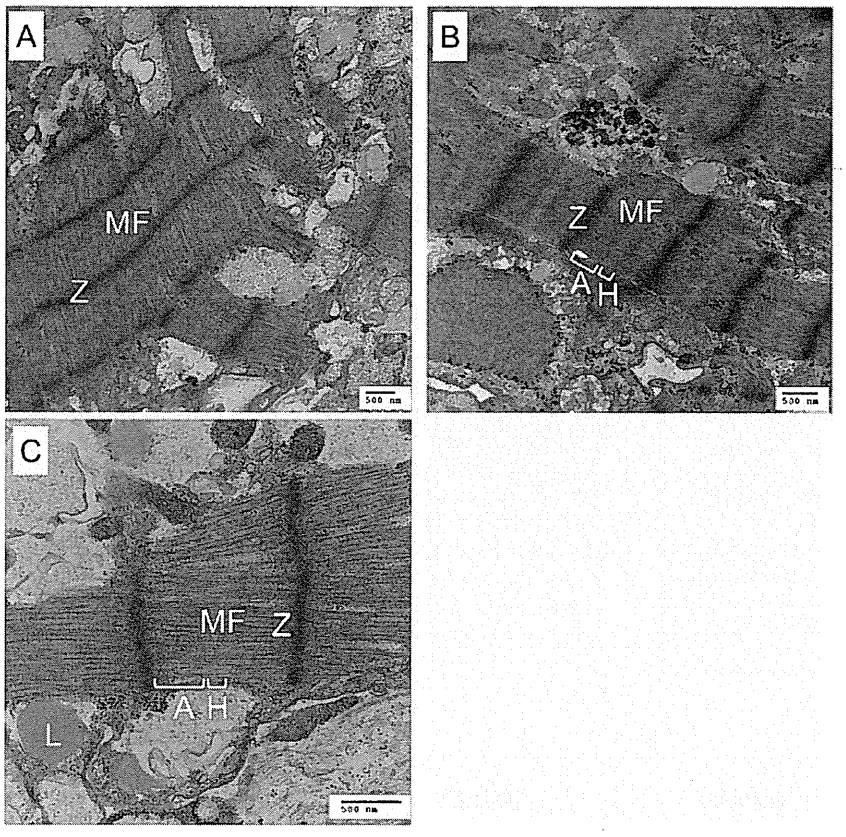

Figure 5. Transmission electron microscopy images of human-induced pluripotent stem cell-derived cardiomyocytes (hiPSC-CMs) at 60 (**A**), 90 (**B**), and 180 days (**C**) after cardiac differentiation. Between 60- and 180-day differentiation, ultrastructural maturation continued and formation of H-bands (H) can be seen. However, even at 180-day differentiation, M-bands are not apparent. Lipid droplets (L) can be seen in (**C**).

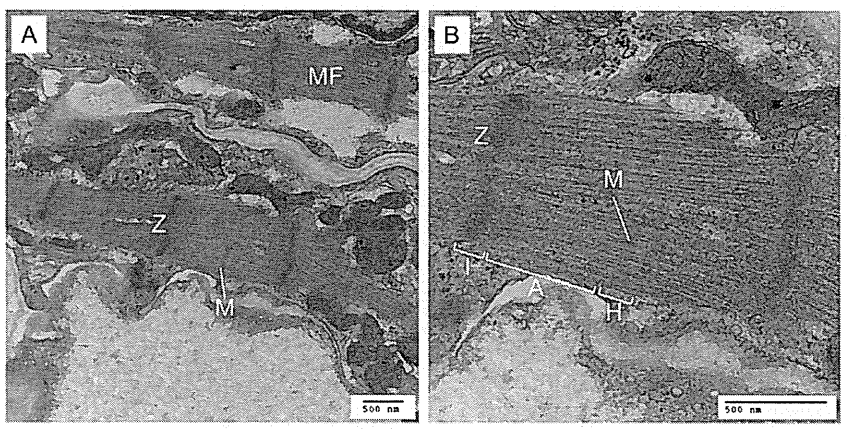

Figure 6. Transmission electron microscopy images of human-induced pluripotent stem cell-derived cardiomyocytes (hiPSC-CMs) at 360 days after cardiac differentiation. (**A**,**B**) In addition to discrete A-, H-, I-, and Z-bands, M-bands (M) are also noted in a minority of the cells within the sarcomeres.

noted in which myofibrils were held between a few of the Z-bands (**Figure 3**). However, A-, H-, I-, and M-bands were not recognized. CMs were connected by desmosomes and fascia adherens at this early stage.

At 30-day differentiation, nascent myofibrils decreased and appeared to be packed between Z-bands. Parallel Z-bands were demonstrated to confine the myofibrils in the typical sarcomeric pattern. Some myofibrils showed A- and I-bands. However, they still lacked the formation of H-, and M-bands (**Figure 4**). Mitochondria and rough endoplasmic reticulum were also noted, as previously reported.[13]

Between 60- and 90-day differentiation, ultrastructural maturation continued and formation of H-bands could be observed. However, even at 180-day differentiation, M-bands could not be detected (**Figure 5**).

Finally, at 360-day differentiation, in addition to discrete A-, H-, I-, and Z-bands, M-bands were first noted in a minority of the cells within the sarcomeres (**Figure 6**). Myofibrils appeared to be tightly packed and distributed in an oriented fashion. The amount of sarcomeric structure in a single CM continued to increase, but was still scarce compared with an adult CM. Even at this stage, different degrees of organization

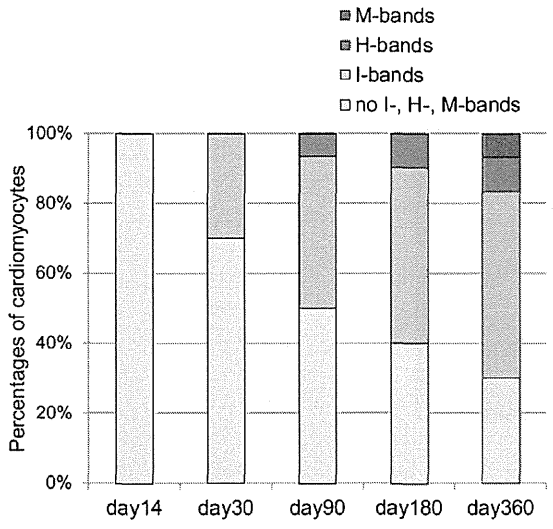

Figure 7. Percentages of the cardiomyocytes (CMs) having I-, H-, and M-bands at 14, 30, 90, 180, 360 days after cardiac differentiation. The amount of CMs with I- and H-bands increased through the long-term culture and M-bands were first noted in 360-day CMs.

existed simultaneously in the same EB.

We evaluated 30 CMs with sarcomeres on randomly selected electron micrographs to assess the maturation process of sarcomeres quantitatively. **Figure 7** shows the percentages of CMs having I-, H-, and M-bands at 14-, 30-, 90-, 180-, 360-day differentiation.

Expression of Cardiac-Specific Genes

Leucine-rich repeat-containing protein 39 (*LRRC39*), myomesin 1 (*MYOM1*), and 2 (*MYOM2*), components of M-bands,[18] increased at 360-day differentiation compared with 30-day differentiation, supporting the observation of M-band formation in 360-day hiPSC-CMs (**Figure 8**). However, the expression levels of the M-band-specific proteins in the hiPSC-CMs were lower compared with those of the adult heart. The expression of cardiac troponin-T (*cTnT*), myosin heavy chain 6 (*MYH6*), myosin heavy chain 7 (*MYH7*), and myosin regulatory light chain 2 (*MYL2*) also increased after the 1-year culture. However, the expression levels of cardiac-specific genes in the hiPSC-CMs were also considerably lower than those in the adult heart left ventricle or left atrium, and in the fetal heart. The expression levels of gap junction α-1 protein were significantly decreased in 180-day and 360-day hiPSC-CMs compared with 30-day hiPSC-CMs.

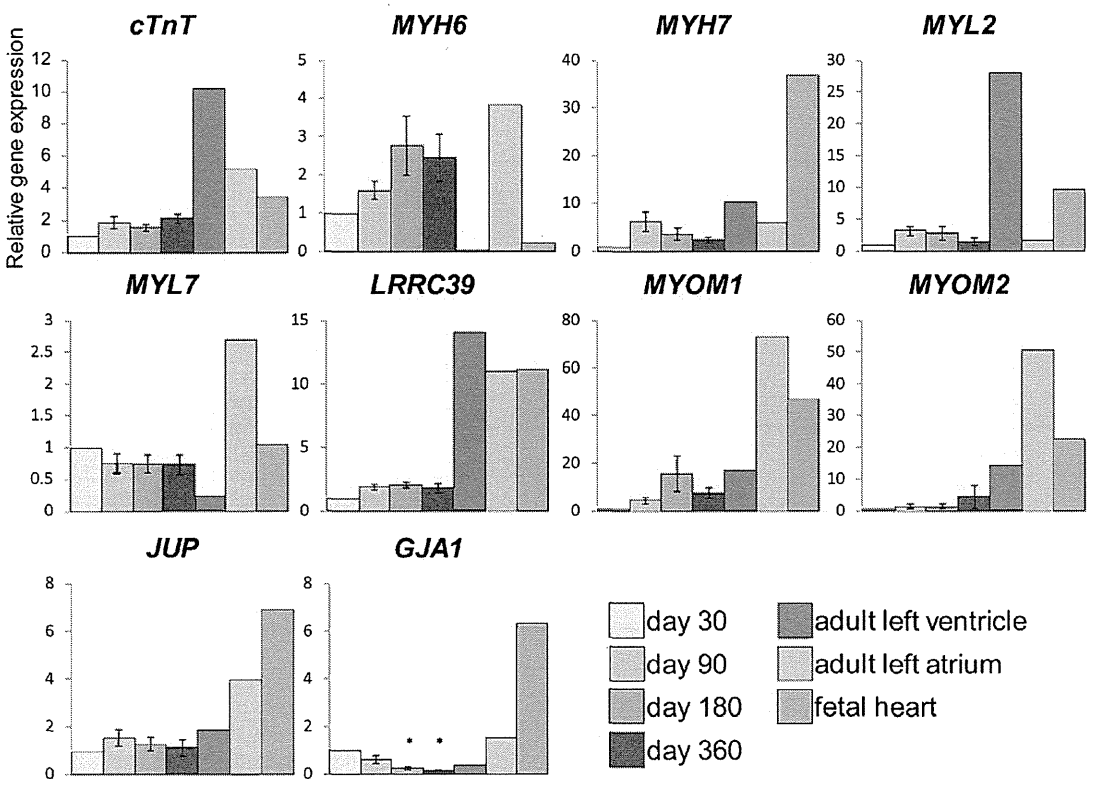

Figure 8. Real-time quantitative polymerase chain reaction analyses for *cTnT*, *MYH6*, *MYH7*, *MYL2*, *MYL7*, *LRRC39*, *MYOM1*, *MYOM2*, *JUP*, and *GJA1* expression in beating embryoid bodies (EB) from human-induced pluripotent stem cell-derived cardiomyocytes (hiPSC-CMs) at 30, 90, 180, and 360 days, in the adult left ventricle, adult left atrium, and fetal heart. The changes in gene expression levels were compared with those of hiPSC-CMs at 30-day differentiation. *cTnT*, cardiac troponin-T; *MYH6*, myosin heavy chain 6; *MYH7*, myosin heavy chain 7; *MYL2*, myosin regulatory light chain 2; *MYL7*, myosin regulatory light chain 7; *LRRC39*, leucine-rich repeat-containing protein 39; *MYOM1*, myomesin 1; *MYOM2*, myomesin 2; *JUP*, junction plakoglobin; *GJA1*, gap junction α-1 protein. *P<0.05 vs. 30-days EBs.

Discussion

In this study, we demonstrated that hiPSC-CMs continue to mature through a 1-year culture. This is the first report of the feasibility of 1-year 2D culture of hiPSC-CMs and description of the sarcomeric maturation process represented by the emergence of M-bands and the increase in the cardiac-specific gene expressions.

So far, the reported ultrastructure of hiPSC-CMs has been immature and their maturation process remained unknown.[4,13,14] Human embryonic stem cell-derived cardiomyocytes (hESC-CMs) are reported to follow a roughly similar maturation process to that reported both in vivo and in an in-vitro murine ES model.[19-24] The hiPSC-CMs in the present study showed a similar maturation process to that of hESC-CMs.[25] At first, narrow, diffusely distributed, and frequently not well aligned myofibrils, resembling those of hiPSC-CMs at 14 days, developed into sarcomeres with clear band patterns including the Z-, I-, and A-bands, responding to hiPSC-CMs at between 30 and 90 days, and ultimately resulted in the generation of well-designed sarcomeres with A-, H-, I-, and M-bands. The ultrastructural findings of hiPSC-CMs in the literature now available relate to around 30 days of differentiation, and only Z- and I-bands have been visible.[4,13,14] In our study, the 30-day hiPSC-CMs similarly showed only Z- and I-bands, not H- or M-bands. Notably, we are the first to find that only 360-day hiPSC-CMs, not 180-day hiPSC-CMs, show a mature sarcomeric structure with M-bands. However, even at 360-day differentiation, different degrees of organization patterns existed simultaneously in the same EB and homogeneous maturation was not confirmed. Our 1-year culture system was able to confirm more mature sarcomeric structures than previously reported, but still not that of adult CMs. It is reported that human CMs derived from fetal hearts do not achieve full ultrastructural maturity and that myofibrillar development continues throughout the entire fetal period.[22] The insufficient maturation of hiPSC-CMs after long-term culture could be explained by several factors. In vitro culturing conditions lack the presence of adjacent non-myocyte proliferating cells, which play an important role in the maturation of CMs via paracrine and humoral signals in vivo. In addition, the CMs grown in the absence of hemodynamic workload typical of in vivo working CMs are reported to lack appropriate ultrastructural development.[26] The differences between in vitro and in vivo conditions, such as the absence of humoral factors and organized mechanical and electrical stress in vitro, might result in delayed ultrastructural maturation.

In electron micrographs of the sarcomere, the M-band appears as a series of parallel electron-dense lines in the central zone of the A-band. The M-band has been reported to play a role not only in mechanical stability in the activated sarcomere, such as reducing the intrinsic instability of thick filaments and helping titin to maintain order in sarcomeres, but also in the biomechanical conditions in contracting muscle such as stress sensing.[27] M-band formation was confirmed in the latest stage and has been considered the endpoint of myofibrillar maturation.[18,21] The lower expression levels of the M-band-specific proteins in the hiPSC-CMs compared with the adult heart might be associated with the delayed appearance of M-bands. Maturation of iPSC-CMs is critical for their application in regenerative medicine, as well as for investigating the mechanisms underlying inherited cardiac diseases. Techniques to promote the maturation of ESC-CMs, such as 3D culture methodology,[28] electric stimulation,[29] and coculture with non-cardiomyocytes[30] may be applicable to iPSC-CMs to overcome the problem, although it has not been fully investigated in hiPSC-CMs. Improved methods are needed to produce homogeneous, mature iPSC-CMs.

In addition to ultrastructural maturation, there was a significant increase in the size of hiPSC-CMs after long-term culture, supporting the process of morphological maturation. Also, the lower rate of beating of 360-day hiPSC-CMs compared with 30-day hiPSC-CMs suggested electrophysiological maturation, because it has been reported that the resting membrane potential becomes progressively more negative in the developing atrial and ventricular myocytes, which correlates with an increasing presence of I_{K1}, and ultimately, the fetal atrial and ventricular myocytes exhibit stable resting membrane potentials with little automaticity.[31]

Changes in the expression patterns of MLC2v and MLC2a occur during the maturation process.[32] hiPSC-CMs were thought to be immature and similar to human fetal CMs because of the presence of a number of MLC2v/MLC2a double-positive CMs.[33] Our immunostaining analysis demonstrated that the percentage of MLC2v/MLC2a double-positive hiPSC-CMs decreased after long-term culture, accompanied by an increase in MLC2v-positive/MLC2a-negative hiPSC-CMs, suggesting maturing of the ventricular-type CMs.

This study also showed for the first time, changes in the expression levels of cardiac-specific genes and genes related to intercalated discs throughout the 1-year culture. The cardiac-specific genes tended to increase during 1-year culture, supporting the maturation process of hiPSC-CMs. The connexin (gap junction proteins) are reported to be more abundant in the neonate than the adult.[34] The significant decrease in *GJA1* expression levels in 180- and 360-day hiPSC-CMs compared with 30-day hiPSC-CMs also suggested maturation of hiPSC-CMs.

Study Limitations

We used microdissected beating EBs for the gene expression studies. The fact that EBs contain CMs at various stages of differentiation, as well as non-CMs, might obscure the results of the gene expression studies. We conducted immunostaining analysis of single cells from microdissected beating EBs 3 days after enzymatic dispersion, which might allow non-CMs to increase and affect the results of the percentage of CMs in the beating EBs.

Conclusions

The current study demonstrated developmental changes in the ultrastructural, immunocytological, and gene expression properties of hiPSC-CMs. Our results confirmed mature sarcomeric structure with M-band formation in long-term culture of hiPSC-CMs for the first time, which provides a new insight into the maturation process of hiPSC-CMs. For application of homogeneous mature hiPSC-CMs in regenerative medicine and in vitro modeling of human cardiac diseases, further maturation of cardiac cells will be needed.

Acknowledgments

We thank Aya Umehara, Masako Tanaka, Kyoko Yoshida, and the Division of Electron Microscopic Study, Center for Anatomical Studies, Kyoto University Graduate School of Medicine for technical assistance.

Sources of Funding

This work was supported by research grants from the Ministry of Education, Culture, Science, and Technology of Japan (T.M. and M.H.), Suzuken Memorial Foundation (T. Kimura), Fujiwara Memorial Foundation

(T.M.), the Uehara Memorial Foundation (M.H.), and health science research grants from the Ministry of Health, Labor and Welfare of Japan for Clinical Research on Measures for Intractable Diseases (T.M. and M.H.).

Disclosures

None.

References

1. Takahashi K, Tanabe K, Ohnuki M, Narita M, Ichisaka T, Tomoda K, et al. Induction of pluripotent stem cells from adult human fibroblasts by defined factors. *Cell* 2007; **131:** 861–872.
2. Zhang J, Wilson GF, Soerens AG, Koonce CH, Yu J, Palecek SP, et al. Functional cardiomyocytes derived from human-induced pluripotent stem cells. *Circ Res* 2009; **104:** e30–e41.
3. Moretti A, Bellin M, Welling A, Jung CB, Lam JT, Bott-Flügel L, et al. Patient-specific induced pluripotent stem-cell models for long-QT syndrome. *N Engl J Med* 2010; **363:** 1397–1409.
4. Novak A, Barad L, Zeevi-Levin N, Shick R, Shtrichman R, Lorber A, et al. Cardiomyocytes generated from CPVT^{D307H} patients are arrhythmogenic in response to β-adrenergic stimulation. *J Cell Mol Med* 2012; **16:** 468–482.
5. Choi SH, Jung SY, Kwon SM, Baek SH. Perspectives on stem cell therapy for cardiac regeneration. *Circ J* 2012; **76:** 1307–1312.
6. Zwi L, Caspi O, Arbel G, Huber I, Gepstein A, Park IH, et al. Cardiomyocyte differentiation of human-induced pluripotent stem cells. *Circulation* 2009; **120:** 1513–1523.
7. Germanguz I, Sedan O, Zeevi-Levin N, Shtrichman R, Barak E, Ziskind A, et al. Molecular characterization and functional properties of cardiomyocytes derived from human inducible pluripotent stem cells. *J Cell Mol Med* 2011; **14:** 38–51.
8. Ma J, Guo L, Fiene SJ, Anson BD, Thomson JA, Kamp TJ, et al. High purity human-induced pluripotent stem cell-derived cardiomyocytes electrophysiological properties of action potentials and ionic currents. *Am J Physiol Heart Circ Physiol* 2011; **301:** H2006–H2017.
9. Tanaka T, Tohyama S, Murata M, Nomura F, Kaneko T, Chen H, et al. In vitro pharmacologic testing using human-induced pluripotent stem cell-derived cardiomyocytes. *Biochem Biophys Res Commun* 2009; **385:** 497–502.
10. Xi J, Khalil M, Shishechian N, Hannes T, Pfannkuche K, Liang H, et al. Comparison of contractile behavior of native murine ventricular tissue and cardiomyocytes derived from embryonic or induced pluripotent stem cells. *FASEB J* 2010; **24:** 2739–2751.
11. Kuzmenkin A, Liang H, Xu G, Pfannkuche K, Eichhorn H, Fatima A, et al. Functional characterization of cardiomyocytes derived from murine induced pluripotent stem cells in vitro. *FASEB J* 2009; **23:** 4168–4180.
12. Jonsson MK, Vos MA, Mirams GR, Duker G, Sartipy P, de Boer TP, et al. Application of human stem cell-derived cardiomyocytes in safety pharmacology requires caution beyond hERG. *J Mol Cell Cardiol* 2012; **52:** 998–1008.
13. Gherghiceanu M, Barad L, Novak A, Reiter I, Itskovitz-Eldor J, Binah O, et al. Cardiomyocytes derived from human embryonic and induced pluripotent stem cells: Comparative ultrastructure. *J Cell Mol Med* 2011; **15:** 2539–2551.
14. Fujiwara M, Yan P, Otsuji TG, Narazaki G, Uosaki H, Fukushima H, et al. Induction and enhancement of cardiac cell differentiation from mouse and human-induced pluripotent stem cells with cyclosporine-A. *PLoS One* 2011; **6:** e16734.
15. Yoshida Y, Takahashi K, Okita K, Ichisaka T, Yamanaka S. Hypoxia enhances the generation of induced pluripotent stem cells. *Cell Stem Cell* 2009; **5:** 237–241.
16. Dubois NC, Craft AM, Sharma P, Elliott DA, Stanley EG, Elefanty AG, et al. SIRPA is a specific cell-surface marker for isolating cardiomyocytes derived from human pluripotent stem cells. *Nat Biotechnol* 2011; **29:** 1011–1018.
17. Yang L, Soonpaa MH, Adler ED, Roepke TK, Kattman SJ, Kennedy M, et al. Human cardiovascular progenitor cells develop from a KDR$^+$ embryonic-stem-cell-derived population. *Nature* 2008; **453:** 524–528.
18. Will RD, Eden M, Just S, Hansen A, Eder A, Frank D, et al. Myomasp/LRRC39, a heart- and muscle-specific protein, is a novel component of the sarcomeric M-band and is involved in stretch sensing. *Circ Res* 2010; **107:** 1253–1264.
19. Beharvand H, Azarnia M, Parivar K, Ashtiani SK. The effect of extracellular matrix on embryonic stem cell-derived cardiomyocytes. *J Mol Cel Cardiol* 2005; **38:** 495–503.
20. Baharvand H, Piryaei A, Rohani R, Taei A, Heidari MH, Hosseini A. Ultrastructural comparison of developing mouse embryonic stem cell- and in vivo-derived cardiomyocytes. *Cell Biol Int* 2006; **30:** 800–807.
21. Anversa P, Olivetti G, Bracchi PG, Loud AV. Postnatal development of the M-band in rat cardiac myofibrils. *Circ Res* 1981; **48:** 561–568.
22. Kim HD, Kim DJ, Lee IJ, Rah BJ, Sawa Y, Schaper J. Human fetal heart development after mid-term: Morphometry and ultrastructural study. *J Mol Cell Cardiol* 1992; **24:** 949–965.
23. Legat MJ. Sarcomerogenesis in human myocardium. *J Mol Cell Cardiol* 1970; **1:** 425–437.
24. Yu L, Gao S, Nie L, Tang M, Huang W, Luo H, et al. Molecular and functional changes in voltage-gated Na^+ channels in cardiomyocytes during mouse embryogenesis. *Circ J* 2011; **75:** 2071–2079.
25. Snir M, Kehat I, Gepstein A, Coleman R, Itskovitz-Eldor J, Livne E, et al. Assessment of the ultrastructural and proliferative properties of human embryonic stem cell-derived cardiomyocytes. *Am J Physiol Heart Circ Physiol* 2003; **285:** H2355–H2363.
26. Bishop SP, Anderson PG, and Tucker DC. Morphological development of the rat heart growing in oculo in the absence of hemodynamic work load. *Circ Res* 1990; **66:** 84–102.
27. Agarkova I, Perriard JC. The M-band: An elastic web that crosslinks thick filaments in the center of the sarcomere. *Trends Cell Biol* 2005; **15:** 477–485.
28. Ou DB, He Y, Chen R, Teng JW, Wang HT, Zeng D, et al. Three-dimensional co-culture facilitates the differentiation of embryonic stem cells into mature cardiomyocytes. *J Cell Biochem* 2011; **112:** 3555–3562.
29. Chen MQ, Xie X, Wilson KD, Sun N, Wu JC, Giovangrandi L, et al. Current-controlled electrical point-source stimulation of embryonic stem cells. *Cell Mol Bioeng* 2009; **2:** 625–635.
30. Kim C, Majdi M, Xia P, Wei KA, Talantova M, Spiering S, et al. Non-cardiomyocytes influence the electrophysiological maturation of human embryonic stem cell-derived cardiomyocytes during differentiation. *Stem Cells Dev* 2010; **19:** 783–795.
31. He JQ, Ma Y, Lee Y, Thomson JA, Kamp TJ. Human embryonic stem cells develop into multiple types of cardiac myocytes: Action potential characterization. *Circ Res* 2003; **93:** 32–39.
32. Kubalak SW, Miller-Hance WC, O'Brien TX, Dyson E, Chien KR. Chamber specification of atrial myosin light chain-2 expression precedes septation during murine cardiogenesis. *J Biol Chem* 1994; **269:** 16961–16970.
33. Mummery CL, Zhang J, Ng ES, Elliott DA, Elefanty AG, Kamp TJ. Differentiation of human embryonic stem cells and induced pluripotent stem cells to cardiomyocytes: A methods overview. *Circ Res* 2012; **111:** 344–358.
34. Allah EA, Tellez JO, Yanni J, Nelson T, Monfredi O, Boyett MR, et al. Changes in the expression of ion channels, connexins and Ca^{2+}-handling proteins in the sino-atrial node during postnatal development. *Exp Physiol* 2011; **96:** 426–438.

Supplementary Files

Supplementary File 1

Table S1. Primer Sequences Used for Real-Time qPCR Analysis

Supplementary File 2

Movie S1. 360-day-old beating embryoid bodies.

Please find supplementary file(s);
http://dx.doi.org/10.1253/circj.CJ-12-0987

ARD Online First, published on December 10, 2013 as 10.1136/annrheumdis-2013-204361

EXTENDED REPORT

Somatic *NLRP3* mosaicism in Muckle-Wells syndrome. A genetic mechanism shared by different phenotypes of cryopyrin-associated periodic syndromes

Kenji Nakagawa,[1] Eva Gonzalez-Roca,[2] Alejandro Souto,[3] Toshinao Kawai,[4] Hiroaki Umebayashi,[5] Josep María Campistol,[6] Jeronima Cañellas,[7] Syuji Takei,[8] Norimoto Kobayashi,[9] Jose Luis Callejas-Rubio,[10] Norberto Ortego-Centeno,[10] Estíbaliz Ruiz-Ortiz,[2] Fina Rius,[2] Jordi Anton,[11] Estibaliz Iglesias,[11] Santiago Jimenez-Treviño,[12] Carmen Vargas,[13] Julian Fernandez-Martin,[14] Inmaculada Calvo,[15] José Hernández-Rodríguez,[16] María Mendez,[17] María Teresa Dordal,[18] Maria Basagaña,[19] Segundo Bujan,[20] Masato Yashiro,[21] Tetsuo Kubota,[22] Ryuji Koike,[22] Naoko Akuta,[23] Kumiko Shimoyama,[24] Naomi Iwata,[25] Megumu K Saito,[26] Osamu Ohara,[27] Naotomo Kambe,[28] Takahiro Yasumi,[1] Kazushi Izawa,[1] Tomoki Kawai,[1] Toshio Heike,[1] Jordi Yagüe,[2] Ryuta Nishikomori,[1] Juan I Aróstegui[2]

Handling editor Tore K Kvien

► Additional material is published online only. To view please visit the journal online (http://dx.doi.org/10.1136/annrheumdis-2013-204361).

For numbered affiliations see end of article.

Correspondence to
Dr Juan I Aróstegui, Immunology Department (esc 4-pl 0), Hospital Clínic, Villarroel, 170, Barcelona 08036, Spain; jiaroste@clinic.ub.es and Dr Ryuta Nishikomori, Department of Pediatrics, Kyoto University Graduate School of Medicine, 54 Shogoin Sakyo, Kyoto 606-8507, Japan; rnishiko@kuhp.kyoto-u.ac.jp

KN, EG-R, RN and JIA contributed equally.

Received 27 July 2013
Revised 16 October 2013
Accepted 24 November 2013

To cite: Nakagawa K, Gonzalez-Roca E, Souto A, *et al. Ann Rheum Dis* Published Online First: [*please include* Day Month Year] doi:10.1136/annrheumdis-2013-204361

ABSTRACT

Familial cold autoinflammatory syndrome, Muckle-Wells syndrome (MWS), and chronic, infantile, neurological, cutaneous and articular (CINCA) syndrome are dominantly inherited autoinflammatory diseases associated to *gain-of-function NLRP3* mutations and included in the cryopyrin-associated periodic syndromes (CAPS). A variable degree of somatic *NLRP3* mosaicism has been detected in ≈35% of patients with CINCA. However, no data are currently available regarding the relevance of this mechanism in other CAPS phenotypes.

Objective To evaluate somatic *NLRP3* mosaicism as the disease-causing mechanism in patients with clinical CAPS phenotypes other than CINCA and *NLRP3* mutation-negative.

Methods *NLRP3* analyses were performed by Sanger sequencing and by massively parallel sequencing. Apoptosis-associated Speck-like protein containing a CARD (ASC)-dependent nuclear factor kappa-light chain-enhancer of activated B cells (NF-κB) activation and transfection-induced THP-1 cell death assays determined the functional consequences of the detected variants.

Results A variable degree (5.5–34.9%) of somatic *NLRP3* mosaicism was detected in 12.5% of enrolled patients, all of them with a MWS phenotype. Six different missense variants, three novel (p.D303A, p.K355T and p.L411F), were identified. Bioinformatics and functional analyses confirmed that they were disease-causing, *gain-of-function NLRP3* mutations. All patients treated with anti-interleukin1 drugs showed long-lasting positive responses.

Conclusions We herein show somatic *NLRP3* mosaicism underlying MWS, probably representing a shared genetic mechanism in CAPS not restricted to CINCA syndrome. The data here described allowed definitive diagnoses of these patients, which had serious implications for gaining access to anti-interleukin 1 treatments under legal indication and for genetic counselling. The detection of somatic mosaicism is difficult when using conventional methods. Potential candidates should benefit from the use of modern genetic tools.

Cryopyrin-associated periodic syndromes (CAPS) are a group of autoinflammatory diseases that include familial cold autoinflammatory syndrome, Muckle-Wells syndrome (MWS), and chronic, infantile, neurological, cutaneous and articular (CINCA) syndrome, also known as neonatal-onset multisystem inflammatory disease (NOMID).[1] Some clinical features are shared by almost all CAPS phenotypes (ie, onset during childhood, an urticaria-like skin rash) whereas others are restricted to certain phenotypes (ie, serum amyloid A protein (AA) amyloidosis in MWS, destructive arthropathy in CINCA-NOMID).[1] CAPS are caused by dominantly inherited or de novo *NLRP3* mutations.[2–4] This gene encodes for cryopyrin, a component of one of the cytosolic complexes named inflammasomes that generate the active form of interleukin 1ß (IL-1ß).[5] Previous studies showed a *gain-of-function* behaviour for those *NLRP3* mutations associated with CAPS because they provoke an uncontrolled IL-1ß overproduction, representing the basis from which to treat these patients with anti-IL-1 drugs.[3 6] Genetic heterogeneity was suggested in CINCA-NOMID because only ≈55% of patients was *NLRP3* mutation-positive.[3 4] The use of novel genetic methods recently detected somatic *NLRP3* mosaicism in ≈35% of patients with CINCA-NOMID.[7 8] However, no data are currently available about the role of this genetic mechanism in other CAPS phenotypes because genetic heterogeneity has hitherto been scarcely reported in previous studies.

We herein show the causal role of somatic *NLRP3* mosaicism in patients with MWS, in whom previous studies did not detect *NLRP3* mutations, suggesting that this genetic mechanism is shared among the different CAPS phenotypes.

PATIENTS AND METHODS

Patients

For this study we enrolled patients with a clinical suspicion of CAPS, with a phenotype of MWS and overlapping syndromes, and *NLRP3* mutation-negative in previous studies. The clinical inclusion criteria were the presence of an urticaria-like skin rash and at least one of the following symptoms: recurrent fever, recurrent arthritis, recurrent aseptic meningitis, sensorineural deafness or AA amyloidosis (see online supplementary table S1 for details). All patients with a CINCA-NOMID phenotype were excluded. The patients' data were collected by direct interviews and chart reviews. Written informed consent from patients (or patients' parents if younger than 18-years-old) was obtained at each institution. The ethics committees of Hospital Clinic, Barcelona and the Graduate School of Medicine, Kyoto University approved this study, which was conducted in accordance with the Helsinki Declaration.

NLRP3 analyses

These analyses were performed in the Graduate School of Medicine, Kyoto University or in the Hospital Clínic, Barcelona. Genomic DNA was obtained from whole peripheral blood using QIAmp DNA Blood Mini Kit (QIAgen, Germany). For Sanger sequencing all exons of *NLRP3* gene were amplified by PCR using the primers and conditions previously described.[2] The PCR amplicons were purified with Illustra ExoStar 1-Step kit (GE Healthcare, USA), bidirectional fluorescence sequencing using ABI BigDye Terminator V.3.1 Cycle Sequencing Kit (Applied Biosystems, USA) and run on an automated ABI 3730XL DNA analyzer. For massively parallel DNA sequencing, all exons of *NLRP3* gene were amplified as previously described.[8] Library preparation and emulsion PCR were performed according to manufacturer's instructions. All sequencing runs were performed on the GS Junior 454 Sequencer using the GS Junior Titanium Sequencing kits (Roche, Switzerland). The obtained sequences were analysed using the Amplicon Variant Analyzer software.

Bioinformatics analyses

In silico sequence analyses were performed using two different algorithms. The Sorting Intolerant from Tolerant is a sequence homology based tool that predicts whether the amino acid substitution is or is not probably damaging by reporting a score. The PolyPhen-2 is a tool for prediction of the possible impact of an amino acid substitution on the structure and function of a protein, and qualitatively appraised as benign, possibly damaging or probably damaging.[9 10]

Functional studies

The functional consequences of the novel *NLRP3* variants were evaluated in two in vitro assays.[11] Wild type and mutant *NLRP3* cDNA, obtained by mutagenesis PCR, were subcloned into the expression vectors pEF-BOSEX and pcDNA5/TO (Invitrogen, USA). The Apoptosis-associated Speck-like protein containing a CARD (ASC)-dependent nuclear factor kappa-light chain-enhancer of activated B cells (NF-κB) activation was evaluated using a dual-luciferase reporter assay in HEK293FT cells transfected with *NLRP3*-pEF-BOSEX plasmids with a NF-kB reporter construct (pNF-kB-luc, BD Biosciences) and an internal control construct (pRLTK, Toyo Ink) in the presence or absence of ASC-expression plasmid. To evaluate the necrosis-like cell death, the THP-1 cell line (a human monocytic cell line derived from a patient with acute monocytic leukemia) was transfected with green fluorescent protein (GFP)-tagged *NLRP3*-pcDNA5/TO plasmids. After 4 h, cells were stained with 7-aminoactinomycin D and cell death of GFP positive cell was analysed by FACS Caliber (Becton-Dickinson).

Statistical analyses

Continuous variables are presented as the mean±SD or as the median and IQR, while categorical variables are presented as numbers, ratios and/or percentages. To detect potential differences among patients with germline mutations and with somatic mutations, the Mann-Whitney U test was used for continuous variables and Fisher's exact test was used for categorical variables.

RESULTS

Genetic analyses

Fifty-six patients (23 Japanese and 33 Spanish) who fulfilled the inclusion criteria were enrolled. Sanger sequencing of the *NLRP3* gene did not identify mutations in any patients. However, small peaks with reduced signal intensities compared with controls were detected in two patients: the A-to-C transversion at c.908 position in Patient 1 and the A-to-G transition at c.1000 position in Patient 2, which encode for the p.Asp303Ala and p.Ile334Val cryopyrin variants, respectively (figure 1A and table 1). Massively parallel DNA sequencing was performed in all patients and revealed somatic *NLRP3* mosaicism in seven patients (7/56; 12.5%). Six different nucleotide changes, all of them located in the exon 3, were detected, and their frequency varied notably among patients, ranging from 5.5% to 34.9% (table 1). All *NLRP3* variants encode for non-synonymous amino acid changes, three of them being novel (p.Asp303Ala, p.Lys355Thr and p.Leu411Phe) and the remainder already described (p.Ile334Val, p.Phe523Leu and p.Glu567Lys) (figure 1B). In Patient 4 the frequency of the mutated *NLRP3* allele remained identical in blood samples obtained over an 8-year period (table 1).

Bioinformatics and functional analyses

All missense *NLRP3* variants were predicted to be possibly or probably damaging to cryopyrin structure and/or function according to at least one of the two algorithms employed, with the only exception of p.Glu567Lys variant (table 1). Interestingly, this *NLRP3* variant was twice detected in the unrelated patients with somatic mosaicism, and has also been reported in other patients with CAPS, reasonably supporting its pathogenic effect.[7 11] We did not find any of the detected *NLRP3* variants in two groups of ethnically matched healthy individuals (Japanese controls n: 200 chromosomes; Spanish controls n: 500 chromosomes) nor in the database National Center for Biotechnology Information (NCBI) single nucleotide polymorphism database (dbSNP) Build 137 (table 1), reasonably ruling out that they could be rare gene polymorphisms.

Finally we evaluated their functional consequences by two different in vitro assays. The results showed that all *NLRP3* variants induced ASC-dependent NF-κB activation (figure 1C) and necrosis-like programmed cell death of THP-1 cell line (figure 1D) at a similar or higher level than those induced by other well-known disease-causing mutations (p.Arg260Trp, p.Asp303Asn and p.Tyr570Cys). Altogether, these data clearly support a pathogenic effect for all *NLRP3* mutations detected as somatic mutations in the enrolled patients.

Clinical features of patients with somatic *NLRP3* mosaicism

At the time of inclusion in the study, the clinical diagnosis of patients with somatic *NLRP3* mosaicism was compatible with MWS. Neither consanguinity nor familial history of the disease

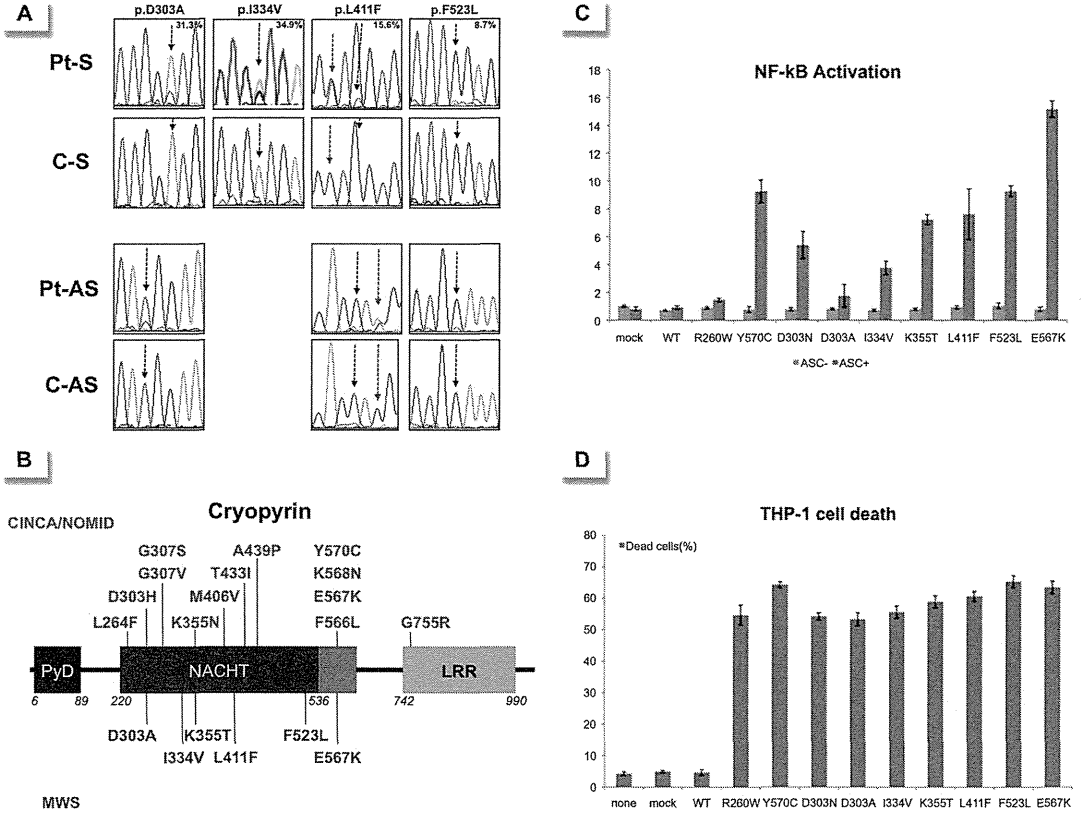

Figure 1 (A) Sense (upper rows) and antisense (bottom rows) chromatograms from four patients with somatic *NLRP3* mosaicism and controls obtained by Sanger sequencing using genomic DNA extracted from whole blood. The black arrows show the *NLRP3* positions where the somatic mutations were detected. The percentage in the upper panels represents the frequency of the mosaicism obtained by massively parallel DNA sequencing in each patient. The red arrows indicate the c.1231 C>T *NLRP3* polymorphism (rs#148478875). (B) Structural organisation of cryopyrin. Above the protein structure are indicated all missense cryopyrin variants that have been detected as somatic mutations in patients with chronic, infantile, neurological, cutaneous and articular (CINCA)-neonatal-onset multisystem inflammatory disease (NOMID) in previous reports, and those below the protein structure are the missense variants detected as somatic mutations in the present study. (C) ASC-dependent NF-kB activation and (D) necrotic THP-1 cell death, induced by the detected *NLRP3* mutations. Values are the mean±SD of triplicate experiments, and data are representative of two independent experiments. AS, antisense; ASC, Apoptosis-associated Speck-like protein containing a CARD; C, control; LRR, leucine-rich repeat; mock, vector without *NLRP3*; MWS, Muckle-Wells syndrome; NACHT, a family of NTPases that originally included the NAIP, CIITA, HETE-E and TP-1 proteins; NF-kB, nuclear factor kappa-light chain-enhancer of activated B cells; None, nothing transfected; Pt, patient; PyD, pyrin domain; S, sense; WT, wild type *NLRP3*.

was reported in any of them. The inflammatory disease started during their infancy or childhood (median: 4 years; IQR: 1.3–9.0 years), with an urticaria-like skin rash and a marked inflammatory acute response as the main features at that time (see table 2 for clinical details at the disease onset).

All patients referred to the chronic course of their disease, with variable disease evolution (median: 20 years; IQR: 12–26 years). During this time, recurrent arthritis (6/7; 85.7%), headache (5/7; 71.4%) and recurrent conjunctivitis (4/7; 57.1%) mainly added to those features detected at the disease onset. None of these patients developed AA amyloidosis, whereas five of them (71.4%) developed progressive bilateral sensorineural deafness (see table 3 for a detailed summary of clinical features detected during the course of the disease).

Outcome of anti-IL-1 blockade

Five patients with somatic *NLRP3* mosaicism were treated with anti-IL-1 drugs. Only Patient 5 was treated with anakinra (100 mg/24 h subcutaneous for a duration of 20 months). Three patients only received canakinumab: Patient 2 (150 mg/8 weeks subcutaneous for a duration of 13 months), Patient 3 (2 mg/kg/8 weeks subcutaneous for a duration of 16 months) and Patient 6 (initial dose of 150 mg/4 weeks, subsequently increased up to 300 mg/4 weeks, for a duration of 14 months). Patient 7 was first treated with anakinra (1 mg/kg/24 h subcutaneous for a duration of 24 months) and subsequently switched to canakinumab (150 mg/8 weeks subcutaneous for a duration of 14 months). All patients showed a marked and sustained improvement while treated with anti-IL-1 drugs, with a complete remission of urticaria-like skin rash (5/5), fever (3/3), conjunctivitis (2/2) and aseptic meningitis (1/1), and marked benefits for arthritis (complete response in 75%) and headache (complete response in 75%, and marked improvement in 25%). Inversely, IL-1 blockade did not improve the sensorineural deafness (0/4). The clinical improvement was associated with sustained reductions of erythrocyte sedimentation rate and C reactive protein level, and normalisation of white blood cell, neutrophil and platelets counts, and haemoglobin level (see figure 2 for details).

Comparative phenotype analyses

To identify potential clinical differences among patients with germline or with somatic *NLRP3* mutations two cohorts of

Table 1 Summary of genetic data of patients with somatic *NLRP3* mosaicism

				Massively parallel DNA sequencing		Bioinformatics analyses				Analysed relatives	
Pt (Country)	Phenotype	Nucleotide exchange*	Amino acid exchange	Mutated allele frequency	Coverage	SIFT	PolyPhen-2	Population genetics†	Reference	Kinship	Results
1 (Spain)	MWS	c.908 A>C	p.D303A	31.3%‡	622×‡	Damaging	Probably damaging	Absent	Present Study	n.d.	n.d.
2 (Japan)	MWS	c.1000 A>G	p.I334V	34.9%‡	1060×‡	Damaging	Benign	Absent	12	Father	Negative§
										Mother	Negative§
3 (Japan)	MWS	c.1064 A>C	p.K355T	20.2%‡	100×‡	Tolerated	Probably damaging	Absent	Present Study	n.d.	n.d.
4¶ (Spain)	MWS	c.[1231 C>T; 1233 G>T]	p.L411F	14.4%‡	590×‡	Tolerated	Possibly damaging	Absent	Present Study	Mother	Negative§
4** (Spain)	MWS	c.[1231 C>T; 1233 G>T]	p.L411F	15.6%‡	870×‡	Tolerated	Possibly damaging	Absent	Present Study	Mother	Negative§
5 (Spain)	MWS	c.1569 C>A	p.F523L	8.7%††	569×††	Tolerated	Possibly damaging	Absent	3	Daughter	Negative§
6 (Japan)	MWS	c.1699 G>A	p.E567K	5.6%‡	1211×‡	Tolerated	Benign	Absent	11	n.d.	n.d.
7 (Japan)	MWS	c.1699 G>A	p.E567K	5.5%‡	724×‡	Tolerated	Benign	Absent	11	n.d.	n.d.

*NCBI Reference Sequence NM_001243133.1.
†Data of population genetics obtained from NCBI dbSNP Build 137.
‡Mean of two independent experiments.
§Analyses performed by Sanger sequencing.
¶Blood sample collected in 2002.
**Blood sample collected in 2009.
††Mean of four independent experiments.
MWS, Muckle-Wells syndrome; n.d., not done; Pt, patient; SIFT, Sorting Intolerant from Tolerant.

patients with MWS were compared. The group of patients with MWS with somatic *NLRP3* mosaicism included the seven patients described here whereas the cohort of patients with MWS with germline mutations included 41 patients (13 Japanese and 28 Spanish) from our databases. In this last group the germline status was established by means of pedigree analyses and/or by massively parallel sequencing. As expected, the familial history of the disease was a significant variable between the two groups. No significant differences were detected among the main clinical features (fever, urticaria-like rash, joint, neurological and ocular involvements, and deafness) despite their variable frequency in each group (see table 4 for details). However, patients with somatic *NLRP3* mosaicism seemed to have late onsets of the disease and of the sensorineural deafness, an increased incidence of arthritis and a reduced risk of developing AA amyloidosis, when compared with patients with germline mutations.

DISCUSSION

CINCA-NOMID syndrome represents the severest CAPS phenotype, and is usually a consequence of de novo *NLRP3* mutations. Recent works have established its genetic basis, with ≈55% of patients carrying germline *NLRP3* mutations and ≈35% carrying somatic *NLRP3* mosaicism.[3–4 7 11–16] However, no studies addressing the presence of somatic *NLRP3* mosaicism have been undertaken in other CAPS phenotypes because genetic heterogeneity has been poorly described in them, with only five reported patients with *NLRP3* mutation-negative MWS.[17–19] This scenario prompted us to hypothesise that somatic *NLRP3* mosaicism might be an underlying genetic mechanism in patients with other CAPS phenotypes. For this proposal two ethnically different cohorts of candidates were screened, and 12.5% of them (7/56) carried variable degree of somatic *NLRP3* mosaicism in peripheral blood. Additional evidences, as shown here, definitively support that the detected *NLRP3* variants are pathogenic

Table 2 Summary of clinical features of patients with somatic *NLRP3* mosaicism at the onset of the disease

Pt	Age at disease onset	Cold-exposure trigger	Urticaria-like skin rash	Fever	Joint involvement	CNS involvement	Acute inflammatory response*	First diagnoses
1	18 years	–	Yes	Yes	Arthralgias	–	Yes	
2	2 years	–	Yes	–	Arthralgias	–	Yes	JIA
3	1 week	–	Yes	–	–	–	Yes	Chronic urticaria, So-JIA
4	14 years	–	Yes	Yes	–	–	Yes	Erythema nodosa
5	4 years	Yes	Yes	Yes	Arthralgias	–	Yes	
6	4 years	Yes	Yes	Yes†	Oligoarthritis	–	Yes	Oligo-JIA
7	7 months	-	Yes	Yes	Oligoarthritis	–	n.a.	So-JIA, TRAPS

*Defined by increased values of white blood cells (normal range 4.00–11.00×10^3/dL), circulating neutrophils (normal range 45–75%), platelets (normal range 130–400×10^3/dL), C reactive protein (normal range <1 mg/dL) and/or erythrocyte sedimentation rate (normal <10 mm/h).
†Low-grade fever.
–, absent; CNS, central nervous system; JIA, juvenile idiopathic arthritis; n.a., not available; Pt, Patient; So-JIA, systemic-onset juvenile idiopathic arthritis; TRAPS, TNF receptor-associated periodic syndrome.

Table 3 Summary of clinical manifestations detected in patients with somatic *NLRP3* mosaicism during the course of the disease

Pt	Sex (Age)	Cold-exposure trigger	Urticaria-like skin rash	Joint involvement					CNS involvement			Deafness (age at onset)	Ocular involvement	AA amyloidosis
				Fever	Type of arthritis	Involved joints	Symmetric	Erosive	Arthropathy	Headache	Aseptic meningitis	Papilloedema			
1	M (39 years)	–	Yes	Yes	Polyarthritis	Large and small	–	–	–	–	–	–	Yes (38 years)	Conjunctivitis	–
2	M (14 years)	–	Yes	–	–	–	–	–	–	Yes	Yes	–	Yes (7 years)	–	–
3	F (12 years)	–	Yes	–	Monoarthritis	Large	–	–	–	Yes	–	–	Yes (6 years)	–	–
4	F (41 years)	–	Yes	Yes	Polyarthritis	Small	–	–	–	Yes	–	–	–	Conjunctivitis	–
5	M (64 years)	Yes*	Yes	Yes†	Polyarthritis	Large and small	–	–	–	–	–	–	Yes (45 years)	–	–
6	F (16 years)	Yes†	Yes	Yes	Oligoarthritis	Large	–	–	–	Yes	–	–	–	Conjunctivitis	–
7	M (16 years)	–	Yes	Yes	Oligoarthritis	Large	–	–	–	Yes	–	–	Yes (13 years)	Conjunctivitis	–

*Always.
†Occasionally.
–, No or absent; AA, serum amyloid A protein; CNS, central nervous system; F, female; M, male; Pt, Patient.

and include their absence in panels of ethnically matched controls and in a database of genomic diversity, in silico analyses that predict their damaging effect for the function and/or structure of cryopyrin, and in vitro functional studies that clearly showed its *gain-of-function* behaviour. Taken together these evidences support that somatic *NLRP3* mosaicism is a genetic mechanism shared by different CAPS phenotypes, and it is not restricted to CINCA-NOMID syndrome.

Among *NLRP3* mutations detected 50% (3/6) were novel, representing an unexpected high proportion for a small cohort. Taking into account their consequences on the cryopyrin function it is conceivable to hypothesise that, in germline status, they could be incompatible with life. We have also found a marked variability in the degree of somatic mosaicism among patients, which may have important consequences. For diagnostic purposes the level of somatic mosaicism could be the determining factor in achieving a definitive genetic diagnosis. Those patients with mosaicism around, or higher than, 15% will probably be detected in conventional studies using Sanger's method by means of careful analyses, as we have shown in the patients' chromatograms. However, those patients with frequencies of less than 15% are probably missed by Sanger sequencing and will only be detected by using new technologies that are not currently widely available. The differences of disease severity observed among patients with somatic mosaicism, including those from this study and those from previous reports, could be explained by different and cumulative factors, which probably cannot be independently analysed. These factors might include, at least, the type of amino acid exchange, its location in the cryopyrin, its functional consequence in the normal cryopyrin function, and the degree and tissue distribution of somatic mosaicism. We must also note that all known somatic *NLRP3* mutations seem to be located in some few amino acid residues (303, 355, 567) or in small regions of cryopyrin (303–307, 433–439 and 566–570), probably representing hot spots for these types of mutations. Consequently these regions should be carefully analysed when using Sanger sequencing to identify potential carriers of somatic mosaicism.

All patients with somatic *NLRP3* mosaicism were sporadic patients, with no affected relatives, which is notably different from patients with germline mutations (positive familial history in 65.9%). Their main clinical features were compatible with a MWS phenotype and similar to those previously described in patients with germline mutations, with the potential exceptions of a reduced incidence of AA amyloidosis, an increased incidence of recurrent arthritis, and slightly older ages at the disease onset and also at onset of sensorineural deafness. It is interesting to note that most patients (4/7; 57.1%) were misdiagnosed as having juvenile idiopathic arthritis when the disease started, a similar misdiagnosis previously reported in different inherited autoinflammatory diseases.[20–23] Despite the evidence shown here, the actual frequency of somatic *NLRP3* mosaicism is unknown and probably underestimated. In our study a potential bias in the selection of patients could exist because they were selected on the basis of the presence of an urticaria-like skin rash associated with other symptoms. Recent studies have described atypical CAPS presentations in patients with germline *NLRP3* mutations in whom urticaria-like skin rash was nearly absent.[24 25] These data suggest that clinical diversity of CAPS is probably wider than previously described and further studies are necessary to delineate the profile of potential candidates to carry somatic *NLRP3* mosaicism.

The evidence obtained may have serious implications for patients, especially with regards to treatment and genetic

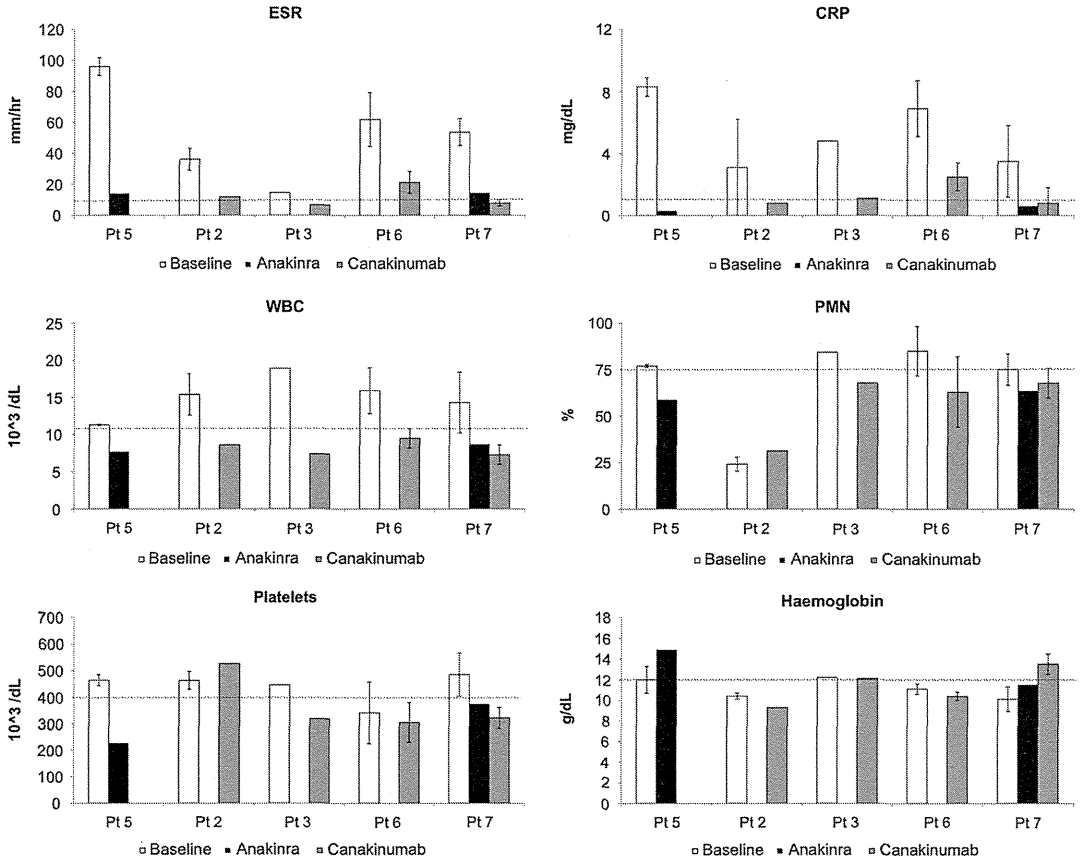

Figure 2 Laboratory values obtained in the five patients treated with different anti-interleukin 1 drugs. Patient's graphics were ordered as follows: First, those graphics from the patient who only received treatment with anakinra (Pt 5), followed by those from patients who only received treatment with canakinumab (Pt 2, 3 and 6) and finally those from the patient who received both treatments (Pt 7). Vertical bars represent the mean±SD of values obtained during treatment periods. Horizontal discontinued lines represent the upper limit of the normal range, with the only exception of the haemoglobin box, in which this line represents the lower limit of the normal range. CRP, C reactive protein; ESR, erythrocyte sedimentation rate; PMN, polymorphonuclears; WBC, white blood cell count.

Table 4 Comparison of main clinical data of patients carrying germline versus somatic *NLRP3* mutations

Clinical features	Patients with germline *NLRP3* mutations (n:41)	Patients with somatic *NLRP3* mutations (n:7)	p Value
Age at disease onset (years)—median (IQR)	0.5 (0.0–4.4)	4.0 (1.3–9.0)	n.s. (p=0.223)
Delay of diagnosis (years)—median (IQR)	33.0 (10–49)	20 (12–26)	n.s. (p=0.416)
Presence of familial history of the disease (%)	65.9	0	p=0.002
Cold exposure as disease triggering factor (%)	36.6	28.6	n.s. (p=1.000)
Fever (%)	63.4	71.4	n.s. (p=1.000)
Urticaria-like skin rash (%)	87.8	100	n.s. (p=1.000)
Joint involvement			
Arthralgias (%)	80.5	85.7	n.s. (p=1.000)
Arthritis (%)	53.7	85.7	n.s. (p=0.214)
Neurological involvement			
Headache (%)	56.1	71.4	n.s. (p=0.683)
Aseptic meningitis (%)	29.3	14.3	n.s. (p=0.656)
Papilloedema (%)	12.2	0	n.s. (p=1.000)
Ocular involvement			
Conjunctivitis (%)	61.0	57.1	n.s. (p=1.000)
Uveitis (%)	17.1	0	n.s. (p=0.573)
Sensorineural deafness (%)	68.3	71.4	n.s. (p=1.000)
Age at onset of deafness (years)—median (IQR)	7.0 (5.5–11)	13.0 (7–38)	n.s. (p=0.210)
AA amyloidosis (%)	17.1	0	n.s. (p=0.573)

Patients with germline mutations were carriers of one of the next *NLRP3* mutations: p.R170S (c.508 C>A), p.R260W (c.778 C>T), p.V262A (c.785 T>C), p.D303N (c.907 G>A), p.H312P (c.935 A>C), p.T348M (c.1043 C>T), p.A439T (c.1315 G>A), p.A439V (c.1316 C>T), p.F443L (c.1329 C>G), p.E567A (c.1700 A>C) and p.Y859C (c.2576 A>G).
AA, serum amyloid A protein; n.s., not significant differences.

counselling. The outcome of IL-1 blockade in patients with somatic *NLRP3* mosaicism was nearly identical to those reported in patients with germline mutations.[26 27] The only symptom that did not improve with IL-1 blockade was the sensorineural deafness. In this regard, apparently contradictory responses have been reported, with improvement or amelioration in some patients and no response in others.[14 17 28–30] It has been suggested that the time of evolution of deafness previous to starting anti-IL-1 drugs could be a determining factor for the type of response, but probably additional and unknown factors could also play a role in this particular manifestation. We have also observed a notable delay in gaining access to anti-IL-1 drugs with respect to the disease onset (median: 20 years; IQR: 12–26 years), because these treatments were administered under legal indication once the definitive CAPS diagnosis was established by means of the identification of somatic *NLRP3* mosaicism. Taking into account the excellent response observed to IL-1 blockade, it is reasonable to hypothesise that if this was started earlier it should have provoked the non-appearance of some severe complications such as deafness.

For an appropriate genetic counselling the scenario is extremely different in patients with CAPS with germline or with somatic mutations. In the case of germline mutations, the risk of transmission to future pregnancies is 50%. Inversely, the prediction of the risk of transmission in cases of somatic mosaicism is more complex, because it may vary in the different tissues, it is not usually determined in gonadal tissues, and its detection probably requires new sensitive genetic methods that are not widely available. The vertical transmission of a somatic mutation is an extremely rare event, with only one case recently described in MWS.[31] Consequently, this possibility should be considered during the genetic counselling of these patients, although one of the main messages to patients is that its probability remains low.

We show that somatic *NLRP3* mosaicism underlies MWS and is probably a shared genetic mechanism in different CAPS phenotypes, and not restricted to CINCA/NOMID syndrome. Its detection was achieved by using massively parallel sequencing, and functional studies confirmed the *gain-of-function* behaviour of the detected variants. The detection of somatic mosaicism has had serious clinical implications for patients, including access to treatment under legal indication, adequate follow-up and ensuring appropriate genetic counselling. Further studies are necessary to delineate the clinical phenotype of candidates to looking for somatic mosaicism, in which new sensitive genetic technologies should be used.

Author affiliations
[1]Department of Pediatrics, Graduate School of Medicine, Kyoto University, Kyoto, Japan
[2]Department of Immunology-CDB, Hospital Clínic-IDIBAPS, Barcelona, Spain
[3]Department of Rheumatology, Hospital Universitario de Santiago de Compostela, Santiago de Compostela, Spain
[4]Department of Human Genetics, National Center for Child Health and Development, Tokyo, Japan
[5]Department of General Pediatrics, Miyagi Children's Hospital, Sendai, Japan
[6]Department of Nephrology, Hospital Clínic-IDIBAPS, Barcelona, Spain
[7]Department of Rheumatology, Hospital Universitari Germans Trias i Pujol, Badalona, Spain
[8]Faculty of Medicine, School of Health Sciences, Kagoshima University, Kagoshima, Japan
[9]Department of Pediatrics, School of Medicine, Shinshu University, Matsumoto, Japan
[10]Department of Internal Medicine, Hospital Universitario San Cecilio, Granada, Spain
[11]Department of Pediatric Rheumatology, Hospital Sant Joan de Deu, Esplugues, Spain
[12]Department of Pediatrics, Hospital Central de Asturias, Oviedo, Spain
[13]Department of Rheumatology, Hospital Virgen de la Macarena, Sevilla, Spain
[14]Department of Internal Medicine, Hospital Meixoeiro, Vigo, Spain
[15]Department of Pediatric Rheumatology, Hospital Universitario La Fe, Valencia, Spain
[16]Department of Autoimmune Diseases, Hospital Clínic-IDIBAPS, Barcelona, Spain
[17]Department of Pediatrics, Hospital Universitari Germans Trias i Pujol, Badalona, Spain
[18]Department of Allergy, Hospital Municipal de Badalona, Badalona, Spain
[19]Allergy Unit, Hospital Universitari Germans Trias i Pujol, Badalona, Spain
[20]Department of Internal Medicine, Hospital Vall d'Hebron, Barcelona, Spain
[21]Department of Pediatrics, Okayama University Graduate School of Medicine, Okayama, Japan
[22]Department of Medicine and Rheumatology, Graduate School of Medical and Dental Sciences, Tokyo Medical and Dental University, Tokyo, Japan
[23]Department of Pediatrics, Graduate School of Medicine, University of Tokyo, Tokyo, Japan
[24]Third Internal Medicine Department, Hamamatsu University School of Medicine, Hamamatsu, Japan
[25]Department of Infection and Immunology, Aichi Children's Health and Medical Centre, Obu, Japan
[26]Department of Clinical Application, Center for iPS cell research and application, Kyoto University, Kyoto, Japan
[27]Department of Human Genome Research, Kazusa DNA Research Institute, Kisarazu, Japan
[28]Department of Dermatology, Chiba University Graduate School of Medicine, Chiba, Japan

Acknowledgements The authors thank the patients and their families for their participation in this study.

Contributors KN, TH, JY, RN and JIA designed research, discussed data and wrote the paper. EG-R, ER-O, FR, EI, TY, KI, TK and OO performed genetic and functional investigations, discussed data and reviewed the manuscript. AS, TK, HU, JMC, JC, ST, NK, JLC-R, NO-C, JA, SJ-T, CV, JF-M, IC, JH-R, MM, MTD, MB, SB, MY, TK, RK, NA, KS, NI, MKS and NK provided clinical data and blood samples, discussed data and reviewed the manuscript.

Funding Supported by the Spanish Ministry of Health (FIS PS09/01182), by the Japan's Ministry of Health, Labor and Welfare, and by the Japan's Ministry of Education, Culture, Sports, Science and Technology.

Competing interests None.

Patient consent Obtained.

Ethics approval The ethics committees of Hospital Clinic, Barcelona and the Graduate School of Medicine, Kyoto University approved this study.

Provenance and peer review Not commissioned; externally peer reviewed.

REFERENCES

1 Kastner DL, Brydges S, Hull KM. Chapter 27: Periodic fever syndromes. In: Ochs HD, Smith CI Edvard, Puck JM. eds. *Primary immunodeficiency diseases. A molecular and genetic approach*. 2nd edn. Oxford University Press, 2007:367–89.
2 Hoffman HM, Mueller JL, Broide DH, *et al*. Mutations of a new gene encoding a putative pyrin-like protein causes familial cold autoinflamatory syndrome and Muckle-Wells syndrome. *Nature Genet* 2001;29:301–5.
3 Aksentijevich I, Nowak M, Mallah M, *et al*. De novo CIAS1 mutations, cytokine activation, and evidence of genetic heterogeneity in patients with Neonatal-Onset Multisystem Inflammatory Disease (NOMID). *Arthritis Rheum* 2002;46:3340–8.
4 Feldman J, Prieur AM, Quartier P, *et al*. Chronic Infantile Neurological Cutaneous and Articular Syndrome is Caused by mutations in CIAS1, a Gene Highly Expressed in polymorphonuclear Cells and Chondrocytes. *Am J Hum Genet* 2002;71:198–203.
5 Martinon F, Mayor A, Tschopp J. The inflammasomes: guardians of the body. *Annu Rev Immunol* 2009;27:229–65.
6 Agostini L, Martinon F, Burns K, *et al*. NALP3 forms an IL-1β-processing inflammasome with increased activity in Muckle-Wells autoinflammatory disorder. *Immunity* 2004;20:319–25.
7 Tanaka N, Izawa K, Saito MK, *et al*. High incidence of NLRP3 somatic mosaicism in patients with chronic infantile neurologic, cutaneous, articular syndrome. Results of an International multicenter collaborative study. *Arthritis Rheum* 2011;63:3625–32.
8 Izawa K, Hijikata A, Tanaka N, *et al*. Detection of base substitution-type somatic mosaicism of the NLRP3 gene with >99.9% statistical confidence by massively parallel sequencing. *DNA Res* 2012;19:143–52.
9 Ng PC, Henikoff S. Accounting for human polymorphisms predicted to affect function. *Genome Res* 2002;12:436–46.
10 Ramensky V, Bork P, Sunyaev S. Human non-synonymous SNPs: server and survey. *Nucleic Acids Res* 2002;30:3894–900.

11 Saito M, Nishikomori R, Kambe N, *et al*. Disease-associated CIAS1 mutations induce monocyte death, revealing low-level mosaicism in mutation-negative cryopyrin-associated periodic syndrome patients. *Blood* 2008;111:2132–41.
12 Cuisset L, Jeru I, Dumont B, *et al*. French CAPS study group. Mutations in the autoinflammatory cryopyrin-associated periodic syndrome gene: epidemiological study and lessons from eight years of genetic analysis in France. *Ann Rheum Dis* 2011;70:495–9.
13 Arostegui JI, Lopez Saldaña MD, Pascal M, *et al*. A somatic NLRP3 Mutation as a cause of a Sporadic Case of CINCA/NOMID Syndrome. Novel evidences of the role of low-level mosaicism as pathophysiological mechanism underlying Mendelian inherited diseases. *Arthritis Rheum* 2010;62:1158–66.
14 Neven B, Marvillet I, Terrada C, *et al*. Long-term efficacy of the interleukin-1 receptor antagonist anakinra in ten patients with Neonatal-Onset Multisystem Inflammatory Disease/Chronic Infantile Neurologic, Cutaneous, Articular syndrome. *Arthritis Rheum* 2010;62:258–67.
15 Aróstegui JI, Aldea AI, Modesto C, *et al*. Clinical and genetic heterogeneity among Spanish patients with recurrent autoinflammatory syndromes-associated to CIAS1/PYPAF1/NALP3 gene. *Arthritis Rheum* 2004;50:4045–50.
16 Saito M, Fujisawa A, Nishikomori R, *et al*. Somatic mosaicism of CIAS1 in a patient with Chronic Infantile Neurologic, Cutaneous, Articular syndrome. *Arthritis Rheum* 2005;52:3579–85.
17 Rynne M, Maclean C, Bybee A, *et al*. Hearing improvement in a patient with variant Muckle-Wells syndrome in response to interleukin 1 receptor antagonism. *Ann Rheum Dis* 2006;65:533–4.
18 Kagami S, Saeki H, Kuwano Y, *et al*. A probable case of Muckle-Wells syndrome. *J Dermatol* 2006;33:118–21.
19 Aksentijevich I, Putnam CD, Remmers EF, *et al*. The clinical continuum of cryopyrinopathies. Novel CIAS1 Mutations in North American patients and a new cryopyrin model. *Arthritis Rheum* 2007;56:1273–85.
20 Ohnishi H, Teramoto T, Iwata H, *et al*. Characterization of NLRP3 variants in Japanese cryopyrin-associated periodic syndrome patients. *J Clin Immunol* 2012;32:221–9.
21 Wise CA, Bennett LB, Pascual V, *et al*. Localization of a gene for familial recurrent arthritis. *Arthritis Rheum* 2000;43:2041–5.
22 Kanazawa N, Okafuji I, Kambe N, *et al*. Early-onset sarcoidosis and CARD15 mutations with constitutive nuclear factor-kappaB activation: common genetic etiology with Blau syndrome. *Blood* 2005;105:1195–7.
23 Aróstegui JI, Arnal C, Merino R, *et al*. NOD2 gene-associated pediatric granulomatous arthritis: clinical diversity, novel and recurrent mutations, and evidence of clinical improvement with interleukin-1 blockade in a Spanish cohort. *Arthritis Rheum* 2007;56:3805–13.
24 Verma D, Eriksson P, Sahdo B, *et al*. Two adult siblings with atypical cryopyrin-associated periodic syndrome due to a novel M299V mutation in NLRP3. *Arthritis Rheum* 2010;62:2138–43.
25 Murphy G, Daly M, O'Sullivan M, *et al*. An unusual phenotype in Muckle-Wells syndrome associated with NLRP3 E311K. *Rheumatology* 2011;50:419–20.
26 Hawkins PN, Lachmann HJ, Aganna E, *et al*. Spectrum of clinical features in Muckle-Wells syndrome and response to anakinra. *Arthritis Rheum* 2004;50:607–12.
27 Lachmann HJ, Kone-Paut I, Kuemmerle-Deschner JB, *et al*. Use of canakinumab in the cryopyrin-associated periodic syndrome. *N Engl J Med* 2009;360:2416–25.
28 Mirault T, Launay D, Cuisset L, *et al*. Recovery from deafness in a patient with Muckle-Wells syndrome treated with anakinra. *Arthritis Rheum* 2006;54:1697–700.
29 Kuemmerle-Deschner JB, Tyrrell PN, Koetter I, *et al*. Efficacy and safety of anakinra therapy in pediatric and adult patients with the autoinflammatory Muckle-Wells syndrome. *Arthritis Rheum* 2011;63:840–9.
30 Weegerink NJ, Schraders M, Leijendeckers J, *et al*. Audiometric characteristics of a Dutch family with Muckle-Wells syndrome. *Hear Res* 2011;282:243–51.
31 Jiménez-Treviño S, González-Roca E, Ruiz-Ortiz E, *et al*. First report of vertical transmission of a somatic *NLRP3* mutation in cryopyrin-associated periodic syndromes. *Ann Rheum Dis* 2013;72:1109–10.

Somatic *NLRP3* mosaicism in Muckle-Wells syndrome. A genetic mechanism shared by different phenotypes of cryopyrin-associated periodic syndromes

Kenji Nakagawa, Eva Gonzalez-Roca, Alejandro Souto, et al.

Ann Rheum Dis published online December 10, 2013
doi: 10.1136/annrheumdis-2013-204361

Notes

Genetic correction of *HAX1* in induced pluripotent stem cells from a patient with severe congenital neutropenia improves defective granulopoiesis

Tatsuya Morishima,[1] Ken-ichiro Watanabe,[1] Akira Niwa,[2] Hideyo Hirai,[3] Satoshi Saida,[1] Takayuki Tanaka,[2] Itaru Kato,[1] Katsutsugu Umeda,[1] Hidefumi Hiramatsu,[1] Megumu K. Saito,[2] Kousaku Matsubara,[4] Souichi Adachi,[5] Masao Kobayashi,[6] Tatsutoshi Nakahata,[2] and Toshio Heike[1]

[1]Department of Pediatrics, Graduate School of Medicine, Kyoto University, Kyoto; [2]Department of Clinical Application, Center for iPS Cell Research and Application, Kyoto University, Kyoto; [3]Department of Transfusion Medicine and Cell Therapy, Kyoto University Hospital, Kyoto; [4]Department of Pediatrics, Nishi-Kobe Medical Center, Kobe; [5]Human Health Sciences, Graduate School of Medicine, Kyoto University, Kyoto; and [6]Department of Pediatrics, Hiroshima University Graduate School of Biomedical Sciences, Hiroshima, Japan

ABSTRACT

HAX1 was identified as the gene responsible for the autosomal recessive type of severe congenital neutropenia. However, the connection between mutations in the *HAX1* gene and defective granulopoiesis in this disease has remained unclear, mainly due to the lack of a useful experimental model for this disease. In this study, we generated induced pluripotent stem cell lines from a patient presenting for severe congenital neutropenia with *HAX1* gene deficiency, and analyzed their *in vitro* neutrophil differentiation potential by using a novel serum- and feeder-free directed differentiation culture system. Cytostaining and flow cytometric analyses of myeloid cells differentiated from patient-derived induced pluripotent stem cells showed arrest at the myeloid progenitor stage and apoptotic predisposition, both of which replicated abnormal granulopoiesis. Moreover, lentiviral transduction of the *HAX1* cDNA into patient-derived induced pluripotent stem cells reversed disease-related abnormal granulopoiesis. This *in vitro* neutrophil differentiation system, which uses patient-derived induced pluripotent stem cells for disease investigation, may serve as a novel experimental model and a platform for high-throughput screening of drugs for various congenital neutrophil disorders in the future.

Introduction

Severe congenital neutropenia (SCN) is a rare myelopoietic disorder resulting in recurrent life-threatening infections due to a lack of mature neutrophils,[1] and individuals with SCN present for myeloid hypoplasia with an arrest of myelopoiesis at the promyelocyte/myelocyte stage.[1,2] SCN is actually a multigene syndrome that can be caused by inherited mutations in several genes. For instance, approximately 60% of SCN patients are known to carry autosomal dominant mutations in the *ELANE* gene, which encodes neutrophil elastase (NE).[3] An autosomal recessive type of SCN was first described by Kostmann in 1956,[4] and defined as Kostmann disease. Although the gene responsible for this classical type of SCN remained unknown for more than 50 years, Klein *et al.* identified mutations in *HAX1* to be responsible for this type of SCN in 2007.[5] HAX1 localizes predominantly to mitochondria, where it controls inner mitochondrial membrane potential ($\Delta\psi_m$) and apoptosis.[6,7] Although an increase in apoptosis in mature neutrophils was presumed to cause neutropenia in HAX1 gene deficiency,[5] the connection between *HAX1* gene mutations and defective granulopoiesis in SCN has remained unclear.

To control infections, SCN patients are generally treated with granulocyte colony-stimulating factor (G-CSF); however, long-term G-CSF therapy associates with an increased risk of myelodysplastic syndrome and acute myeloid leukemia (MDS/AML).[8,9] Although hematopoietic stem cell transplantations are available as the only curative therapy for this disease, they can result in various complications and mortality.[4]

Many murine models of human congenital and acquired diseases are invaluable for disease investigation as well as for novel drug discoveries. However, their use in a research setting can be limited if they fail to mimic strictly the phenotype of the human disease in question. For instance, the *Hax1* knock-out mouse is characterized by lymphocyte loss and neuronal apoptosis, but not neutropenia.[10] Thus, it is not a suitable experimental model for SCN. Induced pluripotent stem (iPS) cells are reprogrammed somatic cells with embryonic stem (ES) cell-like characteristics produced by the introduction of specific transcription factors,[11,16] and they may substitute murine models of human disease. It is believed that iPS cell technology, which generates disease-specific pluripotent stem cells in combination with directed cell differentiation, will contribute enormously to patient-oriented research, including disease pathophysiology, drug screening, cell transplantation, and gene therapy.

In vitro neutrophil differentiation systems, which can reproduce the differentiation of myeloid progenitor cells to mature neutrophils, are needed to understand the pathogenesis of SCN better. Recently, we established a neutrophil differentia-

 doi:10.3324/haematol.2013.083873
The online version of this article has a Supplementary Appendix.
Manuscript received on January 9, 2013. Manuscript accepted on August 20, 2013.
Correspondence: heike@kuhp.kyoto-u.ac.jp

tion system from human iPS cells[17] as well as a serum- and feeder-free monolayer hematopoietic culture system from human ES and iPS cells.[18] In this study, we generate iPS cell lines from an SCN patient with *HAX1* gene deficiency and differentiate them into neutrophils *in vitro*. Furthermore, we corrected for the *HAX1* gene deficiency in HAX1-iPS cells by lentiviral transduction with *HAX1* cDNA and analyzed the neutrophil differentiation potential of these cells. Thus, this *in vitro* neutrophil differentiation system from patient-derived iPS cells may be a useful model for future studies in SCN patients with *HAX1* gene deficiency.

Methods

Human iPS cell generation

Skin biopsy specimens were obtained from an 11-year old male SCN patient with *HAX1* gene deficiency.[19] This study was approved by the Ethics Committee of Kyoto University, and informed consent was obtained from the patient's guardians in accordance with the Declaration of Helsinki. Fibroblasts were expanded in DMEM (Nacalai Tesque, Inc., Kyoto, Japan) containing 10% FBS (vol/vol, Invitrogen, Carlsbad, CA, USA) and 0.5% penicillin and streptomycin (wt/vol, Invitrogen). Generation of iPS cells was performed as described previously.[12] In brief, we introduced *OCT3/4, SOX2, KLF4*, and *cMYC* using ecotropic retroviral transduction into patient's fibroblasts expressing mouse *Slc7a1*. Six days after transduction, cells were harvested and re-plated onto mitotically inactive SNL feeder cells. On the following day, DMEM was replaced with primate ES cell medium (ReproCELL, Kanagawa, Japan) supplemented with basic fibroblast growth factor (5 ng/mL, R&D Systems, Minneapolis, MN, USA). Three weeks later, individual colonies were isolated and expanded.

Maintenance of cells

Control ES (KhES-1) and control iPS (253G4 and 201B6) cells were kindly provided by Drs. Norio Nakatsuji and Shinya Yamanaka (Kyoto University, Kyoto, Japan), respectively. These human ES and iPS cell lines were maintained on mitomycin-C (Kyowa Hakko Kirin, Tokyo, Japan)-treated SNL feeder cells as described previously[17] and subcultured onto new SNL feeder cells every seven days.

Flow cytometric analysis

Cells were stained with antibodies as reported previously.[17] Samples were analyzed using an LSR flow cytometer and Cell Quest software (Becton-Dickinson).

Neutrophil differentiation of iPS cells

In a previous study, we established a serum and feeder-free monolayer hematopoietic culture system from human ES and iPS cells.[18] In this study, we modified this culture system to direct neutrophil differentiation. iPS cell colonies were cultured on growth factor-reduced Matrigel (Becton-Dickinson)-coated cell culture dishes in Stemline II hematopoietic stem cell expansion medium (Sigma-Aldrich, St. Louis, MO, USA) containing the insulin-transferrin-selenium (ITS) supplement (Invitrogen) and cytokines. iPS cells were treated with cytokines as follows: bone morphogenetic protein (BMP) 4 (20 ng/mL, R&D Systems) was added for four days and then replaced with vascular endothelial growth factor (VEGF) 165 (40 ng/mL, R&D Systems) on Day 4. On Day 6, VEGF 165 was replaced with a combination of stem cell factor (SCF, 50 ng/mL, R&D Systems), interleukin (IL)-3 (50 ng/mL, R&D Systems), thrombopoietin (TPO, 5 ng/mL, kindly provided by Kyowa Hakko Kirin), and G-CSF (50 ng/mL, also kindly provided by Kyowa Hakko Kirin). Thereafter, medium was replaced every five days.

Dead cell removal and CD45$^+$ leukocyte separation

Floating cells were collected, followed by the removal of dead cells and cellular debris with the Dead Cell Removal kit (Miltenyi Biotec, Bergisch Gladbach, Germany). CD45$^+$ cells were then separated using human CD45 microbeads (Miltenyi Biotec). Cell separation procedures were performed using the autoMACS Pro Separator (Miltenyi Biotec).

Statistical analysis

Statistical analysis was carried out using Student's t-test. $P<0.05$ was considered statistically significant.

Results

Generation of iPS cell lines from an SCN patient with HAX1 gene deficiency

To generate patient-derived iPS cell lines, dermal fibroblasts were obtained from a male SCN patient with a homozygous 256C-to-T transition resulting in an R86X mutation in the *HAX1* gene.[19] These fibroblasts were reprogrammed to iPS cells after transduction with retroviral vectors encoding *OCT3/4, SOX2, KLF4* and *cMYC*,[12] and a total of 11 iPS cell clones were obtained. From these, we randomly selected three clones for propagation and subsequent analyses. One of these clones (HAX1 4F5) was generated with four factors (*OCT3/4, SOX2, KLF4*, and *cMYC*); the remaining clones (HAX1 3F3 and 3F5) were generated with three factors (*OCT3/4, SOX2*, and *KLF4*).[12]

All of these patient-derived iPS cell clones showed a characteristic human ES cell-like morphology (Figure 1A), and they propagated for serial passages in human ES cell maintenance culture medium. Quantitative PCR analysis showed the expression of *NANOG*, a pluripotent marker gene, to be comparable to that of control ES (KhES-1) and iPS (253G4 and 201B6) cells (Figure 1B). Surface marker analysis indicated that they were also positive for SSEA4, a human ES and iPS cell marker (Figure 1C). DNA sequencing analysis verified an identical mutation in the *HAX1* gene in all established iPS cell clones (Figure 1D). The pluripotency of all iPS cell clones was confirmed by the presence of cell derivatives representing all three germ layers by teratoma formation after subcutaneous injection of undifferentiated iPS cells into immunocompromised NOD/SCID/γc^{null} mice (Figure 1E).

To validate the authenticity of iPS cells further, we investigated the expression of the four genes that were used for iPS cell generation. The expression level of all endogenous genes was comparable to control ES and iPS cells. On the other hand, transgene expression was largely undetectable in patient-derived iPS cell clones (*Online Supplementary Figure S1A*). Chromosomal analysis revealed that all patient-derived iPS cell clones maintained a normal karyotype (*Online Supplementary Figure S1B*). Genetic identity was shown by short tandem repeat analysis (*Online Supplementary Figure S1C*).

Taken collectively, these results indicate that iPS cell clones were comprised of good quality iPS cells derived from the somatic cells of an SCN patient with *HAX1* gene deficiency (HAX1-iPS cells).

Maturation arrest at the progenitor level in neutrophil differentiation from HAX1-iPS cells

The paucity of mature neutrophils in the peripheral blood and a maturation arrest at the promyelocyte/myelocyte stage in the bone marrow are characteristic laboratory findings presented in the SCN patients with *HAX1* gene deficiency. To investigate whether our patient-derived iPS cell model accurately replicated this disease phenotype, we assessed neutrophil differentiation from HAX1-iPS cells by using a serum- and feeder-free monolayer culture system[18] with minor modifications (Online *Supplementary Figure S2*).

In this system, we cultured iPS cell colonies on Matrigel-coated dishes in serum-free medium supplemented with several cytokines and obtained hematopoietic cells as floating cells on approximately Day 26 of differentiation. May-Giemsa staining of floating live CD45$^+$ cells derived from normal iPS cells showed that approximately 40% were mature neutrophils (Figure 2A and B). The remaining cells consisted of immature myeloid cells as well as a small number of macrophages. Cells of other lineages such as erythroid or lymphoid cells were not observed. On the other hand, HAX1-iPS cell-derived blood cells contained only approximately 10% mature neutrophils and approxi-

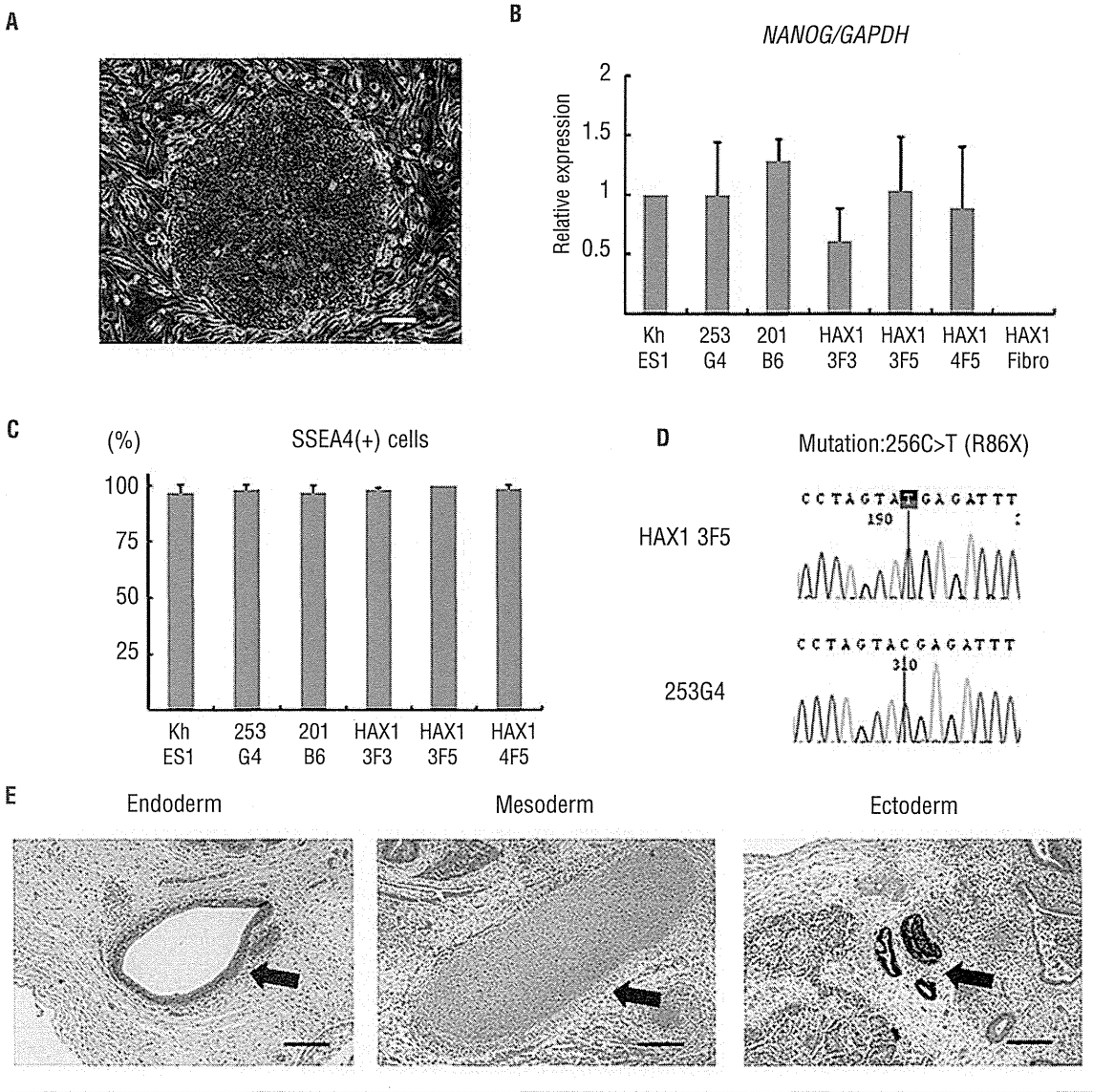

Figure 1. Generation of iPS cell lines from an SCN patient with *HAX1* gene deficiency. (A) Human ES cell-like morphology of HAX1-iPS cells. Scale bar: 200 μm. (B) *NANOG* expression in HAX1-iPS cells, control iPS cells (253G4 and 201B6), and patient-derived fibroblasts (HAX1 Fibro) compared to control ES cells (KhES1). *GAPDH* was used as an internal control (n = 3; bars represent SDs). (C) SSEA-4 expression analysis using flow cytometry. Gated on TRA1-85$^+$DAPI$^-$ cells as viable human iPS (ES) cells (n = 3; bars represent SDs). (D) DNA sequencing analysis of the *HAX1* gene in iPS cells. HAX1-iPS cells showed 256C>T (R86X) mutation that was found in the patient. (E) Teratoma formation from HAX1-iPS cells in the NOD/SCID/γc^{null} (NOG) mouse. Arrows indicate the following; Endoderm: respiratory epithelium; Mesoderm: cartilage; Ectoderm: pigmented epithelium. Scale bars: 200 μm. (A, D-E) Representative data (HAX1 3F5) are shown.